JAIST Repository
https://dspace.jaist.ac.jp/

Title	有機金属構造体を用いた複合膜の調製と水処理への応用
Author(s)	Trinh, Dai Xuan
Citation	
Issue Date	2017-09
Type	Thesis or Dissertation
Text version	ETD
URL	http://hdl.handle.net/10119/14836
Rights	
Description	Supervisor:谷池　俊明，マテリアルサイエンス研究科，博士

JAIST
JAPAN
ADVANCED INSTITUTE OF
SCIENCE AND TECHNOLOGY

Japan Advanced Institute of Science and Technology

Metal-organic framework-based composite membrane and its application to water filtration

TRINH XUAN DAI

Japan Advanced Institute of Science and Technology

Doctoral Dissertation

Metal-organic framework-based composite membrane and its application to water filtration

Trinh Xuan Dai

Supervisor: Associate Professor Toshiaki Taniike

School of Material Science

Japan Advance Institute of Science and Technology

September 2017

Referee-in-chief: Associate Professor Toshiaki Taniike
Japan Advanced Institute of Science and Technology

Referees: Professor Noriyoshi Matsumi
Japan Advanced Institute of Science and Technology

Associate Professor Yuki Nagao
Japan Advanced Institute of Science and Technology

Associate Professor Kazuaki Matsumura
Japan Advanced Institute of Science and Technology

Associate Professor Takashi Morinaga
National Institute of Technology, Tsuruoka College

Table of Contents

Acknowledgement

First of all, I would like to express my profound gratitude to my supervisor – Prof. Toshiaki Taniike for his constant support during 3 years of my doctorial course. I could not study in JAIST without his support, and this thesis would not be accomplished without his patient guidance. I deeply appreciate for his all of efforts devoted in these 3 years.

I would like to thank the Ministry of Education, Cultures, Sports, Science and Technology of Japan for their scholarship during my stay in Japan.

I am also thankful to Prof. Kohki Ebitani for giving me an opportunity to carry out my minor research in his laboratory and providing invaluable suggestions and guidance. Further, I would like to express my thanks to all members of Ebitani laboratory for their help and understanding.

I am thankful for all members of Taniike and Terano laboratories for their sympathy, help and their kindness along the 3 years. They inspired, encouraged and helped me a lot for me to overcome this tense period.

I would like to thank Prof. Takashi Morinaga and his lab members for their kind cooperation.

I would like to acknowledge my colleagues in Faculty of Chemistry, Hanoi University of Science, VNU for helping my vacancy I left during 3 years of the course. I am thankful for my all friends in JAIST for their friendship and kind assistance.

Finally, I would like to thank my family members for their love, taking care and encouraging me for finishing my thesis.

Trinh Xuan Dai

Chapter 1

General introduction

1.1. Shortage of clean water and relevant technologies

Water is world's most specious resource for life. However, the combination of population growth, industrialization and climate change has caused the water shortage problem, and the addressing of the lack of access to clean and safe water is one of the biggest challenges nowadays [1–3]. The high gross domestic product (GDP) growth requires clean water for manufacturing, power generation and domestic zone, which will increase to 400%, 140% and 130% by 2050, respectively. At the same time, the global water demand will increase over 55%, leading to 40% of the world population under the water shortage [4]. In order to match the increase of water demand, the available water resources must be used effectively. Especially, the exploit action of alternative resources such as seawater, brackish ground water and wastewaters will be rational solutions.

For the conventional resources, an emerging problem is the contamination of open water resources such as river and lake water, including the contaminants from municipal, industrial and agriculture waste water. The common contaminants include microorganism, pesticides, pharmaceuticals, heavy metals, industrial chemicals, which can severely affect even at low concentrations. The development of efficient technologies for the removal of these contaminants are very important to provide clean and safe water [5,6].

In this context, the desalination of seawater and brackish water has been considered as the leading technology to overcome the water shortage [4]. The desalination can be classified into two categories: Thermally-driven and membrane-driven (typically reverse osmosis (RO)) types. The conventional thermal-driven technologies, which are based on advanced distillation, evaporation and condensation technologies to obtain fresh water, include multi-stage flash (MSF), multi-effect desalination and adsorption desalination, in which the MSF is the most commonly used. According to the report of Desaldata, MSF,

occupies 21% in total world desalination capacity in 2014 [7]. The advantages of this technology are mainly at its robust operation and independence on feed water quality. However, high production cost, high emission of CO_2 and hot water discharge are the disadvantages of this technique, which leads to the substitution of MSF by the RO technology worldwide. The RO technology is considered as superior to MSF in most of aspects such as unit capital cost, cost of water, CO_2 emission, environmental impact, footprint and so on. For example, the capital costs for RO and MSF are 1313 and 1598 USD/m^3/day, respectively; the water cost of RO technology is at least two times lower; the CO_2 emission (kg/m^3) is estimated as 1.7-2.8 and 15.6-25.0 for RO and MSF, respectively. With these advantages of the RO technology it occupies 65% total world desalination capacity in 2014 [4].

For the RO desalination, the inclusion of other membrane-based processes is highly required. These processes are microfiltration (MF), ultrafiltration (UF) and nanofiltration (NF), which can efficiently reject impurities to reduce the osmotic pressure for the subsequent RO process and elongate the operation time for a RO membrane. Moreover, these processes have been applied for waste water treatment and production of high quality water. In these technologies (RO, NF, UF and MF), membranes as a heart, which determine the efficiency have been continuously developed to improve their performance [8,9]. However, after the invention of the cross-linked thin film polyamide membrane, the development of membrane materials has been almost saturated because of the inherent membrane limitations such as permeability-selectivity tradeoff and fouling propensity. The invention of innovative membrane materials has been expected to solve these problems, which must possess an outstanding water permeability while having a high salt rejection for water purification and desalination technology [10,11].

1.2. Development of membranes

In the publication of "the Sea as a source of fresh water" in 1949, Hassel was the first researcher who studied on a salt rejection using membranes. However, the membrane was not successful in desalination [8]. However, his idea encouraged other researchers. In 1957, Reid and co-workers firstly developed a cellulose diacetate membranes, which showed 96% rejection in the RO application, but the flux was found to be disappointing [12]. In the early 1960s, Loeb-Sourirajan fabricated cellulose diacetate asymmetric membranes. The membranes showed high flux and rejection based on the thin selective layer supported on a porous structure, endowing it with the practical applicability [13]. This is considered as the first breakthrough in membrane-based RO desalination. After that, cellulose triacetate membranes were developed due to its stability in a wider range of temperature and pH as well as higher resistance to chemical and biological fouling as compared to the initial cellulose diacetate. However, the cellulose triacetate membranes were readily compacted, leading to the drop of flux even at moderate pressure of 30 bar [14]. Blending of cellulose diacetate and cellulose triacetate offered a membrane with higher flux and selectivity than the cellulose diacetate membranes. However, the propensity of acetate group to hydrolysis in acidic and alkaline condition limits many practical applications [15]. These drawbacks have motivated the substitution of cellulose acetate membranes by other materials. Although there had been an intense investigation on alternative membrane polymers, cellulose acetate was still the best membrane till 1969 [16].

In 1981, Cadotte reported a high performance membrane using an interfacial polymerization between monomeric amine and monomeric polyacyl halide on porous supports (e.g. polysulfone) [17]. The polymerization occurs on the support membrane at the interface between aqueous amine solution and polyacyl halide in aliphatic solvent,

leading to the formation of ultrathin polyamide layer on the support membrane. The resulting membrane showed high performance in both selectivity and permeability. The next development was devoted to the cross-linking of this polyamide film offering a membrane had five times flux higher than that of the conventional cellulose acetate [18]. Since then, the cross-linked polyamide membranes have been most widely applied in industries instead of the cellulose acetate membranes. It was designed in some different modules such as spiral wound, tubular and hollow fiber to enhance the efficiency of energy consumption.

1.3. Type of membranes

1.3.1. Isotropic membranes

Microporous membranes

A microporous membrane is similar in structure and function to a conventional filter. It has a rigid but highly porous structure in a range of 10 nm to 10 μm. The rejection of a membrane is based on molecular sieving, which is mainly dependent on the molecular size of the filtrate and the pore size distribution of the membrane: A membrane can reject completely particles whose size is greater than that of the largest pores. Particles that are smaller than the largest pore but bigger than the smallest pores partially rejected. The particles are smaller than the smallest pores pass through the membrane. Consequently, the separation is effective only in the case of rejection of significantly different sizes between filtrates and the pore dimension in microfiltration and ultrafiltration [19].

Nonporous, dense membranes

A membrane with a dense thin selective layer on the top, from which permeants are transported by diffusion under the driving force of pressure or concentration gradient. The separation of permeants based on the different transport within the membrane, which is governed by the diffusivity and solubility of each permeant in the membrane. Therefore, these membranes can separate permeants of similar sizes, if their concentration in the membrane is significantly different. Most reverse osmosis membranes are dense membranes, in which the anisotropic structure is designed to improve the permeability of membranes.

1.3.2. Anisotropic membranes

In general, the permeability of membranes is inversely proportional to the thickness of membranes. Indisputably, higher permeability is desired and the thickness of membranes must be as thin as possible. To match this requirement, anisotropic membranes were invented, which not only possess high performance but also exhibit high mechanical strength. These membranes composed of an extremely thin selective layer supported on a much thicker, porous substructure. For example, the thin film composite (TFC) polyamide membrane consists of three layers: A polyester layer acts as a structural support with the thickness of 120-150 µm. An ultra-thin cross-linked polyamide selective layer is usually about 0.2 µm in thickness. Between these layers, a micro-porous interlayer of polysulfone (about 40 µm) is applied to enable the selective layer to withstand high pressure during filtration process [19].

1.4. Membrane processes

There are several membrane processes for desalination and water purification, which are classified mainly based on the solute size. The processes which are driven by hydraulic pressure include microfiltration (MF), ultrafiltration (UF), nanofiltration (NF) and reverse osmosis (RO). Besides, forward osmosis (FO) is an additional process driven by the difference of osmotic pressure between the feed water and a specialized solution of high osmotic pressure (draw solution) (Fig. 1.1).

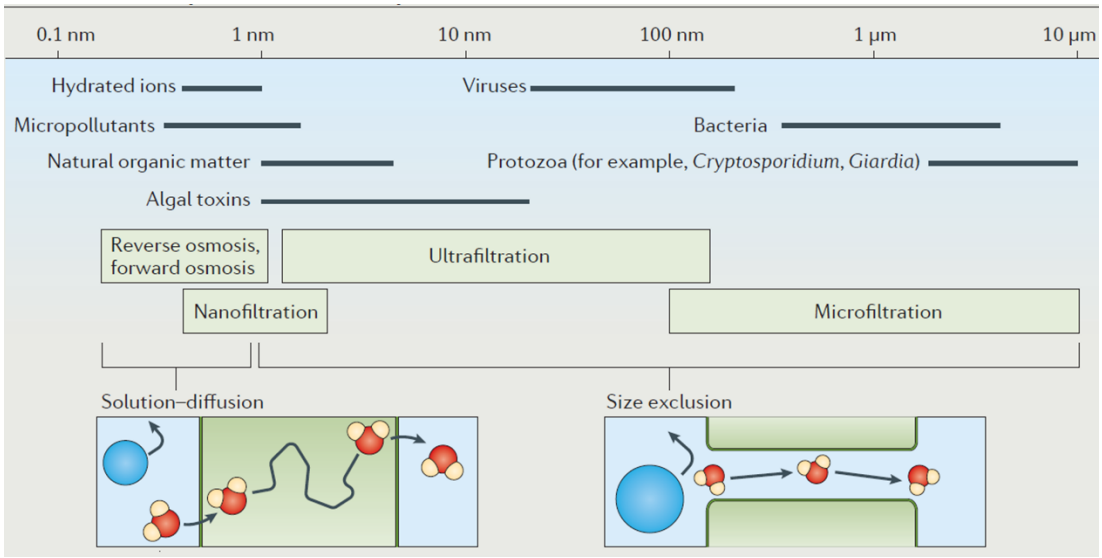

Fig. 1.1. Membrane processes for desalination and water purification. Reproduced from Ref. [11]

MF membranes are used for removal of suspended particles and microbial pathogens. UF membranes are utilized for the rejection of macromolecules and small pathogens such as viruses, which can be removed partially by MF membranes. The molecular-weight cutoff (that is, the molecular size of a solute at which the membrane can reject 90%) of UF membranes lies in the range of 5-500 kDa. MF and UF membranes are porous and the rejection mechanism is based on the size exclusion [20]. NF membranes are designed for the removal of multivalent ions such as Ca^{2+} and Mg^{2+}. The molecular-weight cutoff of NF

membranes is between 100 and 300 Da. RO and FO membranes are designed for desalination and these membranes can reject nearly all ions. The separation of the membranes is based on the diffusion mechanism [21–23], whose details are explained later. The separation of NF membranes is governed by the combination of the sieving and diffusion mechanisms.

1.5. Membrane preparation

1.5.1. Phase inversion technique

Most of the commercial porous membranes used for microfiltration (MF) and ultrafiltration (UF) as well as some dense membranes applied for RO and FO are produced by the phase inversion. This technique involves the transformation of the membrane polymer from one-phase solution into two separate phases by precipitation/solidification (polymer-rich solid phase and polymer-lean liquid phase). The membrane will be formed by casting a solution of membrane polymer on a suitable substrate. The phase inversion technique can be classified into several categories based on the way of solidification from polymer solution [24]:

Non-solvent-induced phase separation (NIPS): This method is the main phase inversion technique, in which polymer dissolved in a solvent is immersed in a non-solvent coagulation bath (typically water), resulting in solvent-non-solvent exchange to cause the precipitation. The solvent and non-solvent must be miscible.

Vapor-induced phase separation (VIPS): The polymer solution is exposed to a non-solvent vapor (often humid air), the adsorption of non-solvent into the polymer solution causes the exchange/precipitation.

Evaporation-induced phase separation (EIPS): The polymer was dissolved in a solvent or in a mixture of a volatile solvent and less volatile non-solvent. The evaporation of a solvent leads to precipitation.

There are some key parameters determining the morphology of resulting membranes. These are the nature of the solvent and non-solvent, the type and concentration of polymer, and so on. In general, due to the stochastic nature of phase inversion technique, leading to a relatively wide pore size distribution, which in turn affects the selectivity of the resulting membrane.

1.5.2. Track-etch technique

In contrast to the phase inversion technique, membranes that are prepared by the track-etch technique possesses an uniform pore size distribution [25]. The pore size of membranes is typically around 10 nm, which can be applied for MF and UF processes. The track-etch technique involves two steps: The first step is the bombardment a polymer film by fission particles from a high-energy source. These particles pass through the film, break polymer chain and create damaged “tracks”. The second step is chemical etching to preferentially etch the tracks for pore formation (Fig. 1.2). Key parameters determining pore density are irradiation intensity and exposure time, whereas the pore size is governed by the etching time. In order to minimize the doublet pore formation when two nucleation tracks are too close, the porosity of the membrane is usually kept relatively low, typically under 10 %. As a result, the flux of the membrane tends to be relatively low.

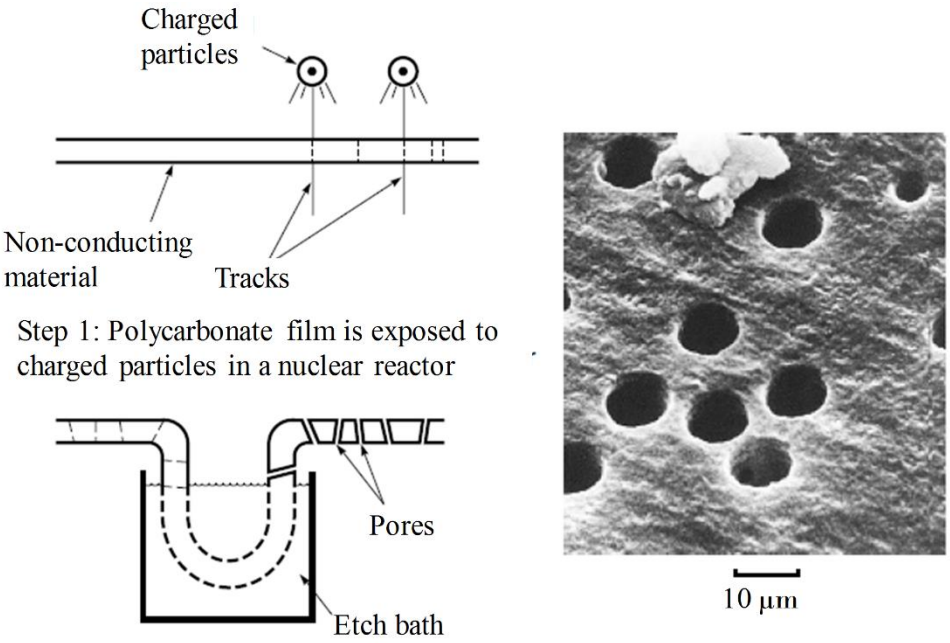

Fig. 1.2. Two steps of track-etch membrane preparation.

1.5.3. Interfacial polymerization technique

The invention of an anisotropic membrane by Loeb and Sourirajan has encouraged the development of numerous techniques, in which a microporous membrane is utilized as a support layer for an ultrathin, dense selective layer. The most successful technique is interfacial polymerization, which was discovered by Cadotte in 1980s. Reverse osmosis membranes produced by this method exhibits remarkable improvement in both salt rejection and permeability in comparison with those of the cellulose acetate RO membrane which was prepared by Loeb and Sourirajan. Since then, almost all NF, RO and FO membranes are made by the interfacial polymerization technique [26–29]. This technique involves the polymerization (often polyamide) at the interface between aqueous and organic phases (typically hexane). A microporous membrane as a support layer was wetted by soaking in aqueous diamine solution (typically 1,3-phenylenediamine). The amine-immersed support is then soaked in an organic phase containing sebacoyl chloride

(nowadays, the most widely used is trimesoyl chloride). The polymerization at the interface forms a dense cross-linked thin selective layer.

It is known that the polymerization occurs in the organic side of the interface. In order to react with trimesoyl chloride, diamine must diffuse through the water-hexane interface to contact with trimesoyl chloride. The reaction cannot occur in aqueous phase because of the limited diffusion of trimesoyl chloride into the aqueous phase. To increase the thickness of the selective layer, amine must continue to pass through the interface, diffuse through the formed polyamide layer to react with an acyl halide in the organic phase. By this way, the thickness increase due to the continuous formation of the polyamide layer.

The composition and morphology of the membrane formed by the interfacial polymerization are known to be dependent on the several parameters such as reaction concentration, partition coefficients of the reactants, the presence of by-products [30–32]. These parameters should be considered to control the formation and properties of the resultant membranes.

1.6. Inherent limitations of membranes

1.6.1. Tradeoff between permeability and selectivity

The water flux *J* through a membrane is defined by

$$J_w = A(\Delta P - \Delta\pi) \qquad (1.1),$$

where A is the water permeability coefficient, and ΔP and $\Delta\pi$ are the applied hydraulic transmembrane and osmotic pressures, respectively. $\Delta\pi$ is negligible for MF and UF processes, while it is significant for NF and RO processes.

In porous membranes, the flow through the selective layer is based on laminar flow through an array of cylindrical pores. Water permeability coefficient is evaluated by the Hagen-Poiseuille equation that includes the surface porosity (ε), pore radius (r_p), solution viscosity (μ) and active layer thickness (δ_m)

$$A = \frac{\varepsilon r_p^2}{8\mu\delta_m} \qquad (1.2).$$

The size distribution of pores influences not only on the flux but also the rejection of the solute in the feed solution. For the solute with the radius of a, the rejection (R) by pores with the radius of r_p ($r_p \geq a$) is given by:

$$R = 1 - \left[2\left(1 - \frac{a}{r_p}\right)^2 - \left(1 - \frac{a}{r_p}\right)^4 \right] \exp\left[-0.7146\left(\frac{a}{r_p}\right)^2 \right] \qquad (1.3).$$

It is clear that the pore size must be smaller than the radius of solute ($r_p \leq a$).

In nonporous membranes, water and solute transport through a selective layer is governed by the solution-diffusion model. The rejection is determined by the difference of diffusion coefficients between water and the solute. The diffusive water permeability (P_w) and diffusive solute permeability (P_s) are related to their solubility and diffusivity in a membrane material, respectively. The water permeability coefficient is determined by [33].

$$A = \frac{P_w V_w}{\delta_m RT} \qquad (1.4),$$

where, V_m is the molar volume of water, R is the gas constant, and T is absolute temperature.

The flux of a solute is determined by the Fick equation as

$$J_s = \frac{P_s}{\delta_m}\Delta c_m = B\Delta c_m \qquad (1.5),$$

where B is the solute permeability coefficient and Δc_m is the difference in the solute concentrations across the selective layer. Both *A* and *B* govern the performance of the selective layer. Perfectly, these coefficients are high to achieve high permeability and selectivity, which are difficult in practical condition. There have been some groups reported that porous and non-porous membranes show a tradeoff between the selectivity and the permeability, which implies that the increase in the permeability is achieved in cost of the significant decrease in the selectivity.

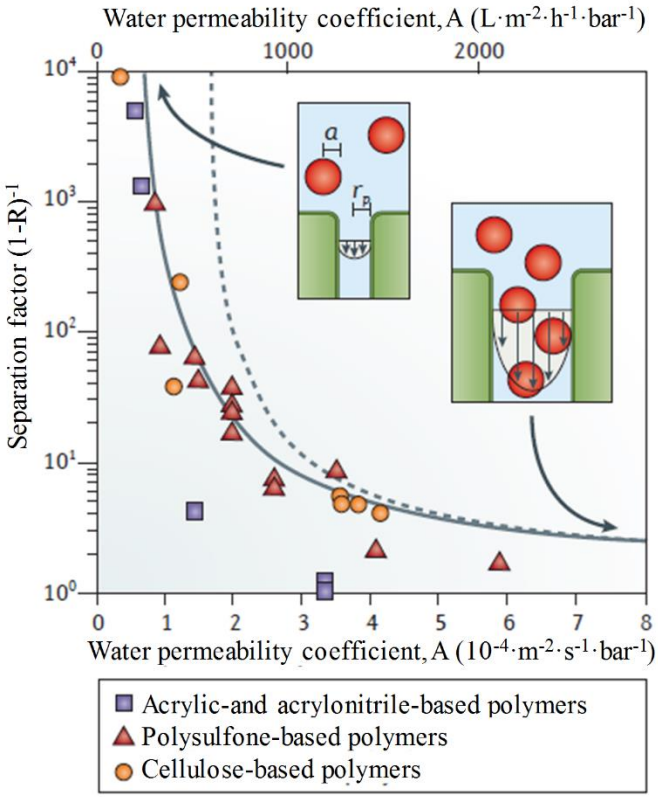

Fig. 1.3. Permeability-selectivity relationship for UF membranes. Reproduced from Ref. [11]

For example, Fig. 1.3 shows the permeability-selectivity tradeoff for UF membranes reject bovine serum albumin. According to Eq. 1.3, the pore size distribution dominates the rejection: An increase in the pore size results in a decrease of the separation factor. Contrary, according to Eq. (1.2), the water permeability increases along the pore size of the selective layer. Therefore, the increase of the pore size of membrane enhances the permeability but reduces the selectivity, as can be depicted in Fig. 1.3. In other sense, if the pore size of the membrane is constant, then from Eq. 1.2, the permeability of the membrane is determined by the thickness and the porosity of the membrane while maintaining the selectivity of the membrane. Because the thickness of the membrane is inversely proportional to the permeability, the best permeability would be achieved with the thinnest membrane thickness.

For the diffusion-solution mechanism, as can be seen in Fig. 1.4, there is an anti-proportional relationship between selectivity and permeability of polymeric membranes in seawater reverse osmosis (SWRO), brackish water reverse osmosis (BWRO) and nanofiltration (NF) [34]. This means that the increase in permeability accompanied by the decrease of selectivity and vise versa. Therefore, at present membrane technology, it is impossible to improve productivity without scarifying water purity in both size exclusion and diffusion-solution mechanisms. In order to match the water demand, this inherent limitation must be addressed.

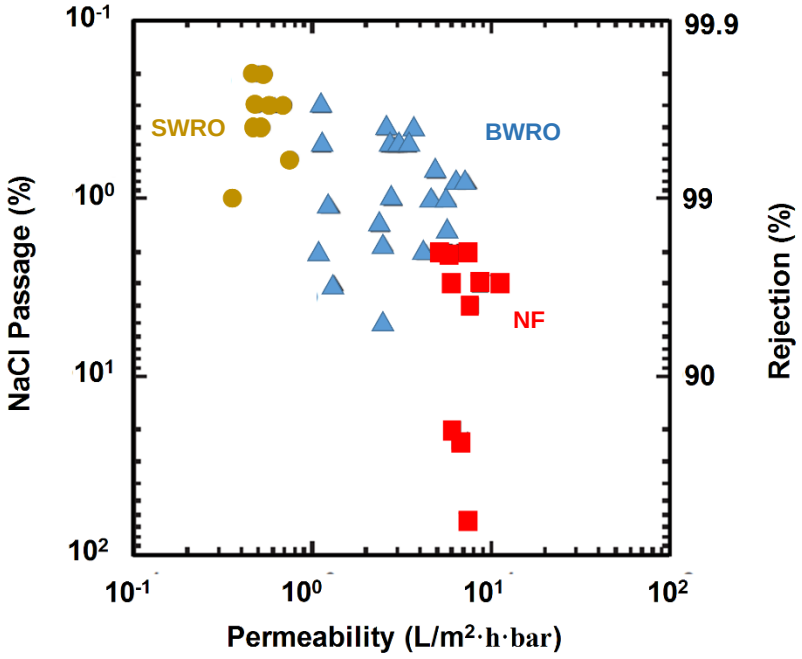

Fig. 1.4. Permeability-selectivity relationship for commercial polymeric membranes. Reproduced from Ref. [34]

1.6.2. Membrane fouling

Membrane fouling is the undesirable accumulation of substances on the surface or/and in the pores of membranes, which deteriorates the membrane performance, especially reduces the flux of membrane [35,36]. In particular, the fouling is a severe problem for membranes used in pressure-driven processes such as MF, UF, NF and RO. In general, the decline of the flux occurs rapidly at the beginning of the fouling (zone I in Fig. 1.5), then the decrease continue slowly (zone II) before reaching a steady state (zone III) [37].

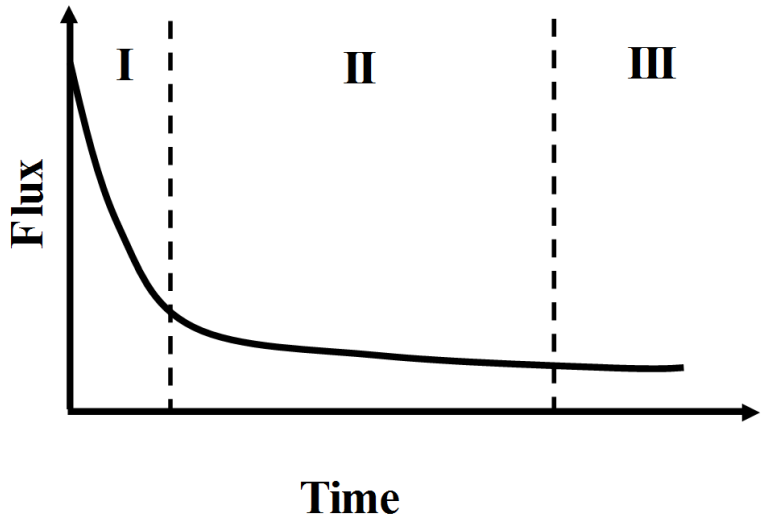

Fig. 1.5. Typical flux decline curve of a membrane caused by fouling

Based on a resistance-in-series model, the permeability decline is caused by four main parameters: membrane hydraulic resistance, concentration polarization resistance, cake layer resistance and adsorption resistance [38–40]. According to these factors, the fouling can be classified into reversible and irreversible fouling. The reversible fouling is caused by cake formation and concentration polymerization, which are easily solved by rinsing steps. While irreversible fouling is caused by foulant adsorption, which cannot be removed by rinsing steps because of the physical interaction and chemical degradation of membrane surfaces by foulants [35].

Based on their characteristics, foulants can be classified into three categories, that are inorganic foulants, organic foulants and biofoulants. Inorganic foulants include precipitates of ions (Fe^{3+}, Mn^{2+}…), which are originally dissolved but precipitated because of oxidation and/or hydrolysis. Organic foulants include dissolved compounds and colloids such as humic acid, proteins, and other hydrophobic materials, which tend to attach to the membrane surface by adsorption. While biofoulants are algae and microorganisms such as bacteria, which adhere to the membrane [36].

There are several factors related to the membrane fouling such as concentration polarization, membrane hydrophobicity, and the roughness of membranes [41–43]. Concentration polarization is the accumulation of a solute near the membrane surfaces due to the rejection of the solute, which in turns facilitates the adsorption of the solute on the membrane surfaces. The common foulants are emulsified oil, microorganisms, protein and humic acid, which are prone to adhere to hydrophobic surfaces rather than to hydrophilic ones. The other factor that also contributes to the membrane fouling is the roughness of the membrane surfaces [44–46]. In literature, rough membrane surfaces show susceptibly to the fouling than the smooth one. For cross-linked polyamide RO membranes, the surface roughness is considered as one of the most important factor for fouling since the membranes are quite hydrophilic.

Based on the above-described parameters on membrane fouling, antifouling strategies have to qualitative considered either to decrease the foulant concentration near the membrane surfaces or to make the membrane surfaces less susceptible to foulants. For the former, there are some techniques such as the pretreatment of feed solution for removing the foulants, and the filtration mode (crossflow) to reduce the foulant near the membrane surfaces. For the latter, a variety of concepts to mitigate the membrane fouling have been proposed, but the most popular one is the modification of membranes to improve their hydrophilicity, which includes blending, grafting and so on [35,36,47].

1.7. New class of materials

1.7.1. Biomimetic membranes

Aquaporins are pore-forming proteins in living cells. They are composed by four identical units, gathering to make one cylindrical channel across bilayer [48]. Theoretical

and experimental results exhibited that aquaporins possess not only exceptionally high permeability but also high solute rejection [49–52]. The structure of aquaporins determines their unique transport properties. As shown in literature, the glass-hour shape of aquaporins consisting of a relatively wide entrances and a narrow center gate, which makes single-file transport of water molecules, leading to exceptionally high water permeability (Fig. 1.6). In terms of the selectivity, aquaporins reject solute based on both their size and charge exslusion. The center gate can adjust to 0.28 nm as a single water molecule, while an arginine side chain offers the constriction site with a positive charge. This tight, charged constriction site prevents charged and neutral solutes from permeation [49–51,53].

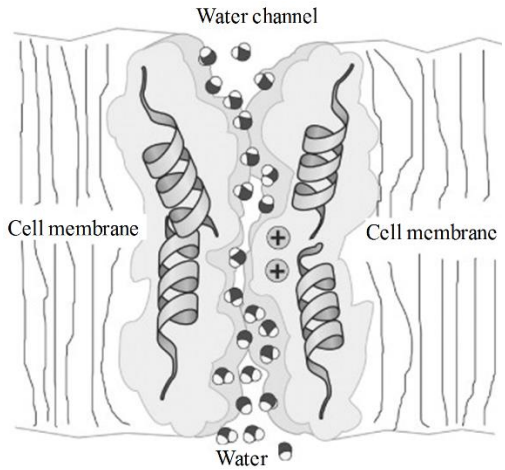

Fig. 1.6. Glass hour structure of aquaporins for water transport. Reproduced form Ref. [52]

The unique combination between high water permeability and high solute rejection of aquaporins has attracted considerable interests over the last decades. A nano-scale membrane was fabricated from aquaporin Z, which exhibited an outstanding permeability of 601 $L \cdot m^{-2} \cdot h^{-1} \cdot bar^{-1}$. This permeability is two orders of magnitudes higher than those of typical commercial RO membranes [54]. There have been several strategies for the fabrication of aquaporin-based membranes for desalination such as the incorporation of

aquaporins in free-standing lipids, or polymer membranes [55–58], stabilization by polymeric support materials [59,60], deposition on a nanofiltration membrane whose wall is negatively charged at pH 7 [61]. In contrast to exceptional permeability, most of these membranes showed very low rejection for NaCl most plausibly because of defects. Most recently, Tang et al. embedded aquaporins in a cross-linked polyamide selective layer by dispersing aquaporins in the aqueous phase before the interfacial polymerization process. The resultant membrane exhibited 96% of NaCl rejection. The permeability of the membrane was 4 $L \cdot m^{-2} \cdot h^{-1} \cdot bar^{-1}$, 40% higher in comparison with that of a commercially available RO membrane [62].

In summary, aquaporin-based membranes are promising for desalination because of the combination between exceptional permeability and high solute rejection. However, these membranes have revealed several limitations including elaborate fabrication, difficulty in scaling-up due to defect formation [63–65]. Moreover, the stability of aquaporin proteins under practical conditions is also a great concern. For example, the activity of microorganisms during continuous use may damage the aquaporins, leading to the instability of the membrane for long-term use.

1.7.2. Carbon nanotubes

Carbon nanotubes (CNTs) have also attracted tremendous interests over the last decades for water purification membranes. Their exceptional properties in water transport were computationally and experimentally studied. Because of their smooth and hydrophobic inner pores, CNTs allow uninterrupted and spontaneous passage of water molecules with negligible adsorption (Fig. 1.7) [66]. A simulation on the application of single-walled (6,6)

CNTs for desalination exhibited the formation of a single-file water wire with ultra-fast water transport. The (6,6) CNTs with the inner diameter of 0.47 nm can completely reject salt, but salt rejection drop dramatically by increasing the diameter. For example, the salt rejection was calculated as only 58% for the inner diameter of 1.1 nm [67].

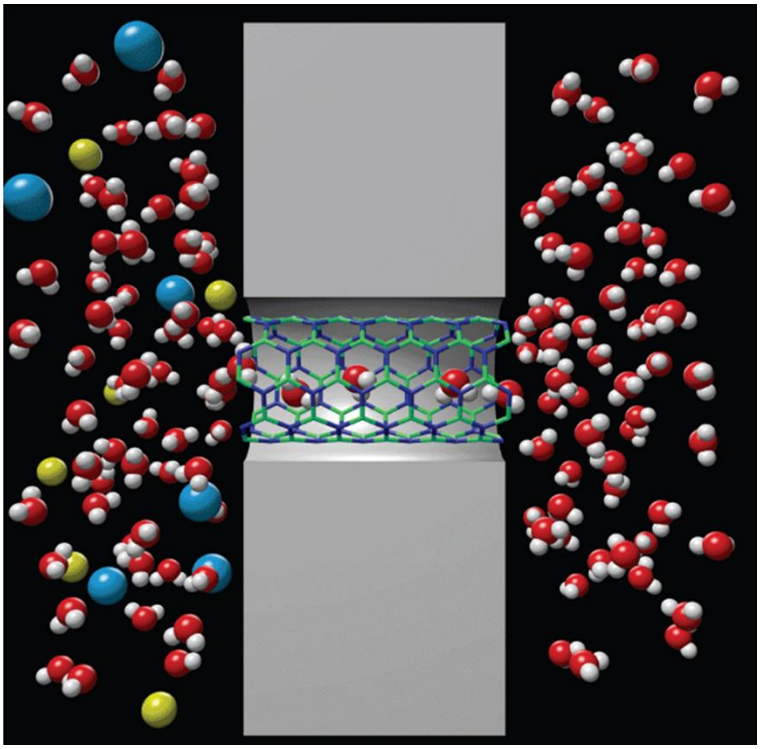

Fig. 1.7. Transport of water molecules through CNTs. Reproduced from Ref. [66]

The dependence of water transport velocity on the diameter of CNTs was also experimentally studied. The investigation of water transport through multi-walled CNTs of 7 nm diameter-embedded in a polystyrene film exhibited that the water velocity passing through the film was four to five orders of magnitudes higher than that of expected value from calculation [68]. In another work, the membrane which incorporated double-walled CNTs with 2 nm diameter provided the water velocity of three to four orders of magnitudes higher than the theoretical estimate [69].

In general, CNTs can be incorporated into membranes in two types; Vertically aligned and mix-matrix CNTs membranes. The former type involves the vertical arrangement of CNTs under the support of polymer, which blocks the water flow to offer only CNTs for permeation and selectivity. The fabrication of such membranes using polystyrene as a host can reject $Ru(NH_3)_6^{3+}$ after functionalization CNT inner wall by negatively charged carboxylate groups [70]. Another report incorporated CNTs in a silicon nitride matrix to form UF membranes. The membranes exhibited a high water flux and 100% rejection Au nanoparticles of 2 nm [69]. In another case, mix-matrix membranes of CNTs offered improved water permeability, solute rejection and mechanical stability. However, the fouling of these membranes was found to be severe [71].

There are several problems which must be addressed in ultilizing CNT-based membranes in practical applications. The inherent size distribution of CNTs causes the low quality in salt rejection, although the permeability may be very outstanding. This drawback limits the application of CNTs for the membranes. The density of CNTs in membranes also need to be taken into account. The close distance of CNTs causes the aggregation, which in turn reduces the homogeneity of the membranes. The use of a suitable host, therefore, plays an important role in deceasing the tendency of agglomeration and keeping the CNTs oriented in the perpendicular direction [71]. The pore size plays a vital role in water desalination. A literature reported that an appropriate pore size for RO membrane is around 0.6 nm to achieve good rejection. Therefore, the diameter of CNTs also should be around 0.6 nm for rational RO applications [72]. In addition, the thickness of membranes is inversely proportional to the water permeability. In order to maintain the exceptional permeability, the thickness must be properly designed [73].

1.7.3. Graphene

Graphene is defined as one layer of carbon atom packed into a honeycomb pattern. As graphene is atomically smooth and thin, it has attracted remarkable interests for membrane separation [74]. The concept of a nanoporous graphene membrane was first mentioned in a simulation study by Cohen and coworkers. In the simulation, the membrane took an advantage of ultrathin graphene (0.35 nm thickness) to form the thinnest selective layer (Fig. 1.8). The simulation proposed that the permeability of the membrane was 1000 $L/m^2 \cdot h \cdot bar$, which was 2-3 time orders of magnitude higher than those of commercial RO membranes. Their research also showed the complete salt rejection when the pores of graphene were as small as 0.27 nm [75]. In the last few years, graphene has been experimentally researched for water desalination. The most recently, Surwade and coworkers successfully fabricated mono layer of graphene by the oxygen plasma etching technique. Nearly complete salt rejection with a very high permeation flux of 250 $L/m^2 \cdot h \cdot bar$ was reported [76]. Although nanoporous graphene layers show an excellent performance in desalination, attaining highly uniform, and sub-nanometer pores at a large scale is a great challenge for such membranes to be appealing in practical application [77].

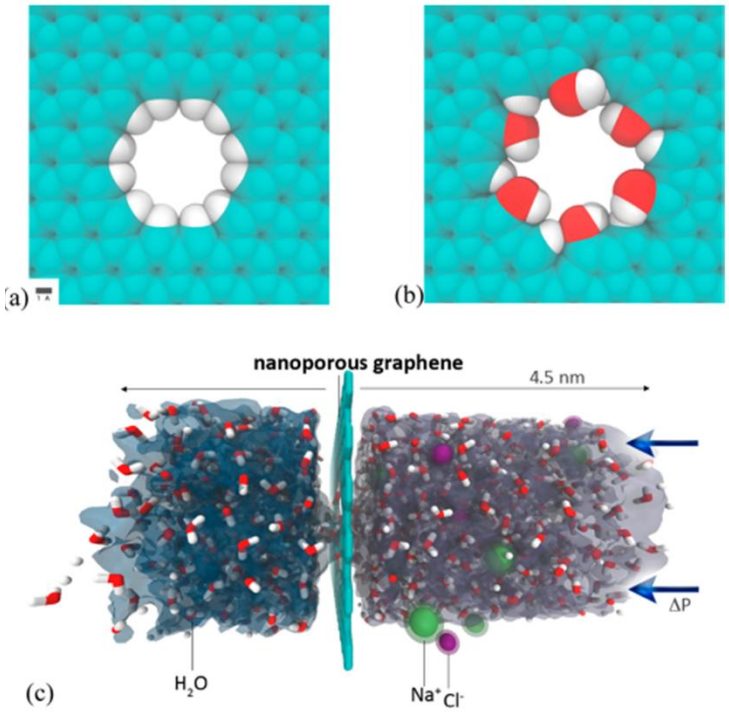

Fig. 1.8. a) Hydrogenated and b) hydroxylated graphene pores, and c) salt rejection by nanoporous graphene. Reproduced from Ref. [75]

Graphene oxide (GO)-based membrane, on the other hand, widely prepared for filtration. GO-based membranes have been typically fabricated by depositing micron-sized GO sheets on porous substrates such as polysulfone (PSf), polyethersulfone (PES) and aluminium oxide (AO) based on vacuum filtration [78], layer-by-layer deposition and so on [79]. Thus prepared selective layer consists of well-packed GO sheets with an intersheet distance of 0.83 nm. When these membranes were immersed into water, GO layers can reject the solutes larger than 0.9 nm in diameter. Hu and Mi fabricated a membrane with cross-linked GO nanosheets deposited on a PSf substrate through a layer-by-layer method. The membrane exhibited a flux 4-10 times higher than those of commercial nanofiltration membranes [78]. In other work, Jiang et al. designed an assembly of crumpled graphene oxide with a vertically tortuous nanochannel membrane. The membrane revealed 400 $L/m^2 \cdot h \cdot bar$ of water permeability for ultrafiltration [80]. Huang et al. incorporated copper

nanostrands of 2.5 nm in diameter among GO sheets. The water permeability was 700 $L/m^2 \cdot h \cdot bar$, 100 times higher than those of commercial membranes [81]. These results suggested that GO is a very promising material for designing performant membranes.

1.7.4. Metal-organic frameworks

Metal-organic frameworks (MOFs), a class of porous crystalline materials, are composed of metal-containing building units and organic linkers. There are several promising advantages of MOFs for separation purposes such as exceptionally high porosity, uniform, easily tunable pore size and well-defined molecular adsorption sites [82–85]. To date, MOFs have been extensively applied to gas separation purposes [82,86,87], while there have been only a handful number of publications on their application to water purification. One of main reasons for this limitation is because of the instability of MOFs in water. It has been reported that many of MOFs are deteriorated their structure in the presence of water and some MOFs even are decomposed with water vapor [88]. However, the said advantages of MOFs for water purification have attracted for water application, especially, after the invention of exceptionally stable zirconium-based MOFs in water.

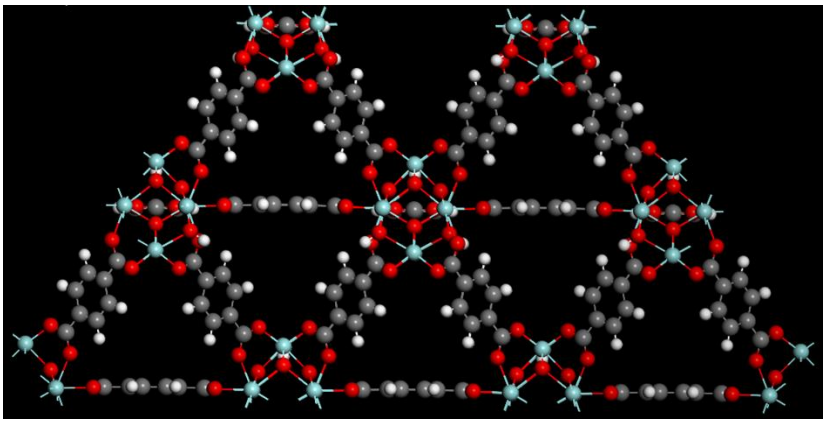

Fig. 1.9. Nanochannel structure of UiO-66

MOF-based membranes have been mainly fabricated by a mix-matrix method, where MOFs were mixed in a solution with a polymer before casting. The presence of MOFs increased the porosity, hydrophilicity of the membranes. Ma et al incorporated UiO-66@GO into polyethersulfone (PES) membranes for ultrafiltration. The inclusion of UiO-66 (Fig. 1.9) increased the hydrophilicity of GO/PES membranes. The flux of the UiO-66@GO/PES membranes was 350% higher than that of PES membranes [89]. In another work, Sotto and coworkers blended MOF-74 with PES before casting membranes. The MOF-based membrane showed the increase of porosity, permeability and antifouling ability compared to the neat PES membrane [90]. By applying the interfacial polymerization, Li et al prepared a ZIF-8 layer on the PES substrate membrane and applied the membrane for ultrafiltration. The incorporation of ZIF-8 significantly enhanced the selectivity of the membranes. However, because of the hydrophobic nature of ZIF-8, the flux of the MOF-based membranes dropped remarkably [91]. More recently, Liu et al deposited UiO-66 on the outermost surface of an alumina hollow fiber by the secondary growth method, a 2 µm thick layer of UiO-66-based membrane can reject multivalent cations from water (98% for Mg^{2+}, 99.3% for Al^{3+}) based on size exclusion mechanism. While the permeability of the membrane was 0.28 ($L/m^2 \cdot h \cdot bar \cdot \mu m$) is same order of magnitude as that of commercial polymeric RO membrane [92]. These promising results suggest that MOFs are emerging as an excellent class of materials.

1.8. Purpose of the thesis

The tradeoff between selectivity and permeability of conventional membranes can be addressed by employing a new class of materials that possess exceptionally high permeability and high selectivity. As mentioned above, this class of materials include

nanochannel-based materials such as aquaporins, CNTs, nanoporous graphene and graphene oxide, which contains nanochannels with diameters size within size of one to two water molecules (0.28 – 0.6 nm). By experimental and computational study, these nanochannel-based materials exhibited permeability from one to several orders of magnitudes higher than those of commercial membranes while achieving high rejection of salt. However, the challenge of these materials is limitation in practical application basically due to the challenge in scaling up these nanochannel-based membranes [11]. For example, nanoporous graphene membrane with hydroxylated pore size of 0.45 nm exhibited a permeability from two to three orders of magnitudes higher than those of commercial membranes. However, the largest such a membrane could be achieved at a 5 μm-diameter membrane [74]. For the other materials, defect-free membranes at larger level have not yet prepared.

MOFs-based membranes, on the other hands, can be prepared in larger scales. MOF-based membranes show the improvement of permeability because of the presence of nanochannel in MOF structure. However, because of harsh reaction condition, in order to prepare such membranes, inorganic substrates are used as support membranes providing non-flexible membranes, which in turn limit in practical application in advanced membrane modules such as spiral wound.

In this research, UiO-66, one of the most stable MOFs to chemicals was utilized for membrane preparation because of its advantages such as hydrophilic nature, pore aperture size of 6 Å which allows the transport of water molecules but struggle hydrated ions. By using this nanochannel-based material, I aim to solve the limitations of conventional membranes. On the other hand, because UiO-66 synthesis requires a hash reaction condition leading to non-flexible membranes. Therefore, I also aim to address the

limitations of previous research by preparing a flexible UiO-66-based membranes in a large scale. To do so, MOF nanoparticles was supported by a commercial polymeric substrate forming a new composite membrane. The porous polymeric substrate provides the flexibility of the composite membrane while a discontinuous MOF selective layer can also offer a flexible layer. The membrane of this research aims to apply for nanofiltration and reverse osmosis desalination.

1.9. References

[1] M. Shannon, P.W. Bohn, M. Elimelech, J.G. Georgiadis, B.J. Mariñas, A.M. Mayes, Science and technology for water purification in the coming decades, Nature 452 (2008) 301–310.

[2] M. Elimelech, The global challenge for adequate and safe water, J. Water Supply Res. Technol. Aqua 55 (2006) 3–10.

[3] Z.E. Hughes, J.D. Gale, A computational investigation of the properties of a reverse osmosis membrane, J. Mater. Chem. 20 (2010) 7788.

[4] M.W. Shahzah, M. Burhan, L. Ang, K.C. Ng, Energy-water-environment nexsus underpinning future desalination sustainability, Desalination 413 (2017) 52–64.

[5] D.W. Kolpin, E.T. Furlong, M.T. Meyesr, E.M. Thurman, S.D. Zaugg, L.B. Barber, H.T. Buxton, Pharmaceuticals, hormones, and other organic wastewater contaminants in U.S. streams, 1999-2000: A national reconnaissance, Environ. Sci. Technol. 36 (2002) 1202–1211.

[6] R.P. Schwarzenbach, B.I. Escher, K. Fenner, T.B. Hofstetter, C.A. Johnson, U.V. Gunten, B. Wehrli, The Challenge of Micropollutants in Aquatic Systems, Science 313 (2006) 1072–1077.

[7] S. Burn, M. Hoang, D. Zarzo, F. Oleniak, E. Campo, B. Bolto, O. Barron, Desalination techniques – A review of the opportunities for desalination, Desalination 364 (2015) 2–16.

[8] K.P. Lee, T.C. Arnot, D. Mattia, A review of reverse osmosis membrane materials for desalination-Development to date and future potential, J. Memb. Sci. 370 (2011)

1–22.

[9] S.S. Shenvi, A.M. Isloor, A.F. Ismail, A review on RO membrane technology: Developments and challenges, Desalination 368 (2015) 10–26.

[10] D.X. Trinh, T. Phuong, N. Tran, T. Taniike, Fabrication of new composite membrane filled with UiO-66 nanoparticles and its application to nanofiltration, Sep. Purif. Technol. 177 (2017) 249–256.

[11] J.R. Werber, C.O. Osuji, M. Elimelech, Materials for next-generation desalination and water purification membranes, Nat. Rev. Mater. (2016) 16018.

[12] C.E. Reid, E.J. Breton, Water and ion flow across cellulosic membranes, J. Appl. Polym. Sci. 1 (1959) 133–143.

[13] S. Loeb, S. Sourirajan, Sea water demineralization by means of an osmotic membrane, Adv. Chem. Series 38 (1962) 117.

[14] R.G. Sudak, Reverse Osmosis, in: M.C. Poter (Ed.) Handbook of Industrial Membrane Technology, Noyes publication, New Jersey, 1990.

[15] W.M. King, P.A. Cantor, L.W. Schoellenback, C.R. Cannon, High retention reverse osmosis desalination membranes from cellulose acetate, in: A.F. Turbak (Ed.), Membranes from Cellulose Derivatives, Interscience Publisher, New York, 1970.

[16] K.J. Edgar, C.M. Buchanan, J.S. Debenham, P.A. Rundquist, B.D. Seiler, M.C. Shelton, D. Tindall, Advances in cellulose ester performance and application, Prog. Polym. Sci. 26 (2001) 1605–1688.

[17] J.E. Cadotte, Interfacially synthesized reverse osmosis membrane, United States Patent 1981.

[18] R.J. Petersen, Composite reverse osmosis and nanofiltration membranes, J. Memb. Sci. 83 (1993) 81–150.

[19] R.W. Baker, Membrane Technology and Applications, Second Ed., John Wiley & Sons Publisher, New York, 2004.

[20] G.M. Geise, H.S. Lee, D.J. Miller, B.D. Freeman, J.E. Macgrath, D.R. Paul, Water Purification by Membranes: The Role of Polymer Science, J. Polym. Sci. Part B. 48 (2010) 1685–1718.

[21] U. Merten, Flow relationship in reverse osmosis, Ind. Eng. Chem. Fundamen. 3 (1963) 229–232.

[22] H.K. Lonsdale, U. Merten, R.L. Riley, J. Jay, Transport Properties of Cellulose Acetate Osmotic Membranes, J. Appl. Polym. Sci. 9 (1965) 1341–1362.

[23] M. Mulder, Basic principles of Membrane Technology, Second Ed., Kluwer Academic Publishers, Dordrecht, The Netherlands, 1996.

[24] H. Susanto, M. Ulbricht, Polymeric Membranes for Molecular Separations, in: E. Drioli & L. Gionor (Ed.) Membrane Operation, Wiley VCH publisher, 2009.

[25] Q. Zhu, Q. Xu, Immobilization of Ultrafine Metal Nanoparticles to High-Surface-Area Materials and Their Catalytic Applications, Chem. 1 (2016) 220–245.

[26] A.P. Korikov, P.B. Kosaraju, K.K. Sirkar, Interfacially polymerized hydrophilic microporous thin film composite membranes on porous polypropylene hollow fibers and flat films, J. Memb. Sci. 279 (2006) 588–600.

[27] B.J. Abu Tarboush, D. Rana, T. Matsuura, H.A. Arafat, R.M. Narbaitz, Preparation of thin-film-composite polyamide membranes for desalination using novel

hydrophilic surface modifying macromolecules, J. Memb. Sci. 325 (2008) 166–175.

[28] S. Veríssimo, K.V. Peinemann, J. Bordado, Influence of the diamine structure on the nanofiltration performance, surface morphology and surface charge of the composite polyamide membranes, J. Memb. Sci. 279 (2006) 266–275.

[29] S.H. Huang, C.L. Li, C.C. Hu, H.A. Tsai, K.R. Lee, J.Y. Lai, Polyamide thin-film composite membranes prepared by interfacial polymerization for pervaporation separation, Desalination 200 (2006) 387–389.

[30] A.K. Ghosh, B.H. Jeong, X. Huang, E.M.V. Hoek, Impacts of reaction and curing conditions on polyamide composite reverse osmosis membrane properties, J. Memb. Sci. 311 (2008) 34–45.

[31] I.J. Roh, A.R. Greenberg, V.P. Khare, Synthesis and characterization of interfacially polymerized polyamide thin films, Desalination 191 (2006) 279–290.

[32] A.P. Rao, N. V. Desai, R. Rangarajan, Interfacially synthesized thin film composite RO membranes for seawater desalination, J. Memb. Sci. 124 (1997) 263–272.

[33] G.M. Geise, D.R. Paul, B.D. Freeman, Fundamental water and salt transport properties of polymeric materials, Prog. Polym. Sci. 39 (2014) 1–24.

[34] G.M. Geise, H.B. Park, A.C. Sagle, B.D. Freeman, J.E. MacGrath, Water permeability and water/salt selectivity tradeoff in polymers for desalination, J. Memb. Sci. 369 (2011) 130–138.

[35] R. Zhang, Y. Liu, M. He, Y. Su, X. Zhao, Antifouling membranes for sustainable water purification : strategies and mechanisms, Chem. Soc. Rev. 45 (2016) 5888–5924.

[36] W. Guo, H. Ngo, J. Li, Bioresource Technology A mini-review on membrane fouling, Bioresour. Technol. 122 (2012) 27–34.

[37] L. Wang, L. Song, Flux decline in crossflow microfiltration and ultrafiltration: Experimental verification of fouling dynamics, J. Memb. Sci. 160 (1999) 41–50.

[38] R.S. Juang, H.L. Chen, Y.S. Chen, Resistance-in-series analysis in cross-flow ultrafiltration of fermentation broths of Bacillus subtilis culture, J. Memb. Sci. 323 (2008) 193–200.

[39] C. Wang, Q. Li, H. Tang, D. Yan, W. Zhou, J. Xing, Y. Wan, Membrane fouling mechanism in ultrafiltration of succinic acid fermentation broth, Bioresour. Technol. 116 (2012) 366–371.

[40] R.S. Juang, H.L. Chen, Y.S. Chen, Membrane fouling and resistance analysis in dead-end ultrafiltration of Bacillus subtilis fermentation broths, Sep. Purif. Technol. 63 (2008) 531–538.

[41] C.Y. Tang, T.H. Chong, A.G. Fane, Colloidal interactions and fouling of NF and RO membranes: A review, Adv. Colloid. Interface Sci. 164 (2011) 126–143.

[42] A.D. Marshall, P.A. Munro, G. Tragardh, The effect of protein fouling in microfiltration and ultrafiltration on permeate flux, protein retention and selectivity: A literature review, Desalination 91 (1993) 65–108.

[43] G. Belfort, R.H. Davis, A.L. Zydney, The behavior of suspensions and macromolecular solutions in crossflow microfiltration, J. Memb. Sci. 96 (1994) 1–58.

[44] Q. Li, Z. Xu, I. Pinnau, Fouling of reverse osmosis membranes by biopolymers in

wastewater secondary effluent: Role of membrane surface properties and initial permeate flux, J. Memb. Sci. 290 (2007) 173–181.

[45] E.M. Vrijenhoek, S. Hong, M. Elimelech, Influence of membrane surface properties on initial rate of colloidal fouling of reverse osmosis and nanofiltration membranes, J. Memb. Sci. 188 (2001) 115–128.

[46] M. Elimelech, X. Zhu, A.E. Childress, S. Hong, Role of membrane surface morphology in colloidal fouling of cellulose acetate and composite aromatic polyamide reverse osmosis membranes, J. Memb. Sci. 127 (1997) 101–109.

[47] D.J. Miller, D.R. Dreyer, C.W. Bielawski, D.R. Paul, B.D. Freeman, Surface Modification of Water Purification Membranes: A Review, Angew. Chem. Int. Ed. 56 (2017) 4662–4711.

[48] M.J. Borgnia, D. Kozono, G. Calamita, P.C. Maloney, P. Agre, Functional reconstitution and characterization of AqpZ, the E. coli water channel protein., J. Mol. Biol. 291 (1999) 1169–79.

[49] E. Beitz, B. Wu, L.M. Holm, J.E. Schultz, T. Zeuthen, Point mutations in the aromatic/arginine region in aquaporin 1 allow passage of urea, glycerol, ammonia, and protons., Proc. Natl. Acad. Sci. 103 (2006) 269–274.

[50] J.S. Hub, B.L. de Groot, Mechanism of selectivity in aquaporins and aquaglyceroporins., Proc. Natl. Acad. Sci. USA 105 (2008) 1198–1203.

[51] H.X. Sui, B.G. Han, J.K. Lee, P. Walian, B.K. Jap, Structural basis of water-specific transport through the AQP1 water channel, Nature 414 (2001) 872–878.

[52] K. Murata, K. Mitsuoka, T. Hirai, T. Walz, P. Agre, J.B. Heymann, A. Engel, Y.

Fujiyoshi, Structural determinants of water permeation through aquaporin-1, Nature 407 (2000) 599–605.

[53] D.F. Savage, J.D. O'Connell, L.J.W. Miercke, J. Finer-Moore, R.M. Stroud, Structural context shapes the aquaporin selectivity filter., Proc. Natl. Acad. Sci. USA 107 (2010) 17164–17169.

[54] C.Y. Tang, Y. Zhao, R. Wang, C. Hélix-Nielsen, A.G. Fane, Desalination by biomimetic aquaporin membranes: Review of status and prospects, Desalination. 308 (2013) 34–40.

[55] A. González-Pérez, K.B. Stibius, T. Vissing, C.H. Nielsen, O.G. Mouritsen, Biomimetic triblock copolymer membrane arrays: A stable template for functional membrane proteins, Langmuir 25 (2009) 10447–10450.

[56] J.S. Hansen, M. Perry, J. Vogel, J.S. Groth, T. Vissing, M.S. Larsen, O. Geschke, J. Emneús, H. Bohr, C.H. Nielsen, Large scale biomimetic membrane arrays, Anal. Bioanal. Chem. 395 (2009) 719–727.

[57] J. Vogel, M. Perry, J.S. Hansen, P.-Y. Bolinger, C.H. Nielsen, O. Geschke, A support structure for biomimetic applications, J. Micromech. Microeng. 19 (2009) 25026.

[58] J.S. Hansen, M. Perry, J. Vogel, T. Vissing, C.R. Hansen, O. Geschke, J. Emnéus, C.H. Nielsen, Development of an automation technique for the establishment of functional lipid bilayer arrays, J. Micromech. Microeng. 19 (2009) 25014.

[59] S. Ibragimova, K. Stibius, P. Szewczykowski, M. Perry, H. Bohr, C. Hélix-Nielsen, Hydrogels for in situ encapsulation of biomimetic membrane arrays, Polym. Adv. Technol. 23 (2012) 182–189.

[60] M. R. Lander, S. Ibragimova, C. Rein, J. Vogel, K. Stibius, O. Geschke, M. Perry, C. Hélix-Nielsen, Biomimetic membrane arrays on cast hydrogel supports, Langmuir 27 (2011) 7002–7007.

[61] Y. Kaufman, A. Berman, V. Freger, Supported lipid bilayer membranes for water purification by reverse osmosis, Langmuir 26 (2010) 7388–7395.

[62] Y. Zhao, C. Qiu, X. Li, A. Vararattanavech, W. Shen, J. Torres, C. Hélix-Nielsen, R. Wang, X. Hu, A.G. Fane, C.Y. Tang, Synthesis of robust and high-performance aquaporin-based biomimetic membranes by interfacial polymerization-membrane preparation and RO performance characterization, J. Memb. Sci. 423–424 (2012) 422–428.

[63] M. Wang, Z. Wang, X. Wang, S. Wang, W. Ding, C. Gao, Layer-by-layer assembly of aquaporin z-incorporated biomimetic membranes for water purification, Environ. Sci. Technol. 49 (2015) 3761–3768.

[64] P.S. Zhong, T.S. Chung, K. Jeyaseelan, A. Armugam, Aquaporin-embedded biomimetic membranes for nanofiltration, J. Memb. Sci. 407–408 (2012) 27–33.

[65] H. Wang, T.S. Chung, Y.W. Tong, K. Jeyaseelan, A. Armugam, Z. Chen, M. Hong, W. Meier, Highly permeable and selective pore-spanning biomimetic membrane embedded with aquaporin Z, Small 8 (2012) 1185–1190.

[66] R. Das, M.E. Ali, S.B.A. Hamid, S. Ramakrishna, Z.Z. Chowdhury, Carbon nanotube membranes for water purification: A bright future in water desalination, Desalination 336 (2014) 97–109.

[67] B. Corry, Designing Carbon Nanotube Membranes for Efficient Water Desalination,

J. Phys. Chem. B 112 (2008) 1427–1434.

[68] M. Majumder, N. Chopra, R. Andrews, B.J. Hinds, Nanoscale Hydrodynamic: Enhanced Flow in Carbon Nanotubes, Nature 438 (2005) 44.

[69] J.K. Holt, H.G. Park, Y. Wang, M. Stadermann, A.B. Artyukhin, C.P. Grigoropoulos, A. Noy, O. Bakajin, Fast mass transport through sub-2-nanometer carbon nanotubes, Science 312 (2006) 1034-1037.

[70] B.J. Hinds, N. Chopra, T. Rantell, R. Andrews, V. Gavalas, L.G. Bachas, Aligned multiwalled carbon nanotube membranes, Science 303 (2004) 62–65.

[71] H.Y. Yang, Z.J. Han, S.F. Yu, K.L. Pey, K. Ostrikov, R. Karnik, Carbon nanotube membranes with ultrahigh specific adsorption capacity for water desalination and purification., Nat. Commun. 4 (2013) 2220.

[72] C.H. Ahn, Y. Baek, C. Lee, S.O. Kim, S. Kim, S. Lee, S.H. Kim, S.S. Bae, J. Park, J. Yoon, Carbon nanotube-based membranes: Fabrication and application to desalination, J. Ind. Eng. Chem. 18 (2012) 1551–1559.

[73] A. Zhu, P.D. Christofides, Y. Cohen, Effect of thermodynamic restriction on energy cost Optimization of RO membrane water desalination, Ind. Eng. Chem. Res. 48 (2009) 6010–6021.

[74] Y. Jiang, P. Biswas, J.D. Fortner, A review of recent developments in graphene-enabled membranes for water treatment, Environ. Sci. Water Res. Technol. 2 (2016) 915–922.

[75] D. Cohen-Tanugi, J.C. Grossman, Water desalination across nanoporous graphene, Nano Lett. 12 (2012) 3602–3608.

[76] S.P. Surwade, S.N. Smirnov, I.V. Vlassiouk, R.R. Unocic, G.M. Veith, S. Dai, S.M. Mahurin, graphene, Nat. Nanotechnol. 10 (2015) 459–464.

[77] D. Cohen-Tanugi, J.C. Grossman, Nanoporous graphene as a reverse osmosis membrane: Recent insights from theory and simulation, Desalination 366 (2015) 59–70.

[78] Y. Han, Y. Jiang, C. Gao, High-flux graphene oxide nanofiltration membrane intercalated by carbon nanotubes, ACS Appl. Mater. Interfaces 7 (2015) 8147–8155.

[79] M. Hu, B. Mi, Enabling Graphene Oxide Nanosheets as Water Separation Membranes, Environ. Sci. Technol. 47 (2013) 3715–3723.

[80] G. Zhao, J. Li, X. Ren, C. Chen, X. Wang, Few-layered graphene oxide nanosheets for heavy metal ion pollution management, Environ. Sci. Technol. 45 (2011) 10454–10462.

[81] H. Huang, Z. Song, N. Wei, L. Shi, Y. Mao, Y. Ying, L. Sun, Z. Xu, X. Peng, Ultrafast viscous water flow through nanostrand-channelled graphene oxide membranes, Nat. Commun. 4 (2013) 2979.

[82] W. Lu, Z. Wei, Z.-Y. Gu, T.-F. Liu, J. Park, J. Park, J. Tian, M. Zhang, Q. Zhang, T. Gentle III, M. Bosch, H.-C. Zhou, Tuning the structure and function of metal–organic frameworks via linker design, Chem. Soc. Rev. 43 (2014) 5561–5593.

[83] H.-C. "Joe" Zhou, S. Kitagawa, Metal–Organic Frameworks (MOFs), Chem. Soc. Rev. 43 (2014) 5415–5418.

[84] S. Qiu, M. Xue, G. Zhu, Metal-organic framework membranes: from synthesis to separation application., Chem. Soc. Rev. 43 (2014) 6116–6140.

[85] N. Yanai, S. Granick, Directional self-assembly of a colloidal metal-organic framework, Angew. Chem. Int. Ed. 51 (2012) 5638–5641.

[86] A. Schaate, P. Roy, A. Godt, J. Lippke, F. Waltz, M. Wiebcke, P. Behrens, Modulated synthesis of Zr-based metal-organic frameworks: From nano to single crystals, Chem. Eur. J. 17 (2011) 6643–6651.

[87] M. Shah, M.C. Mccarthy, S. Sachdeva, A.K. Lee, H. Jeong, Current Status of Metal-Organic Framework Membranes for Gas Separations : Promises and Challenges, Ind. Eng. Chem. Res. 51 (2012) 2179–2199.

[88] N.C. Burtch, H. Jasuja, K.S. Walton, Water Stability and Adsorption in Metal − Organic Frameworks, Chem. Rev. 114 (2014) 10575−10612.

[89] J. Ma, X. Guo, Y. Ying, D. Liu, C. Zhong, Composite ultrafiltration membrane tailored by MOF @ GO with highly improved water purification performance, Chem. Eng. J. 313 (2016) 890–898.

[90] A. Sotto, G. Orcajo, J.M. Arsuaga, G. Calleja, J. L.-Aguirre, Preparation and characterization of MOF-PES ultrafiltration membranes, J. Appl. Polym. Sci. 132 (2015) 41633.

[91] Y. Li, L.H. Wee, A. Volodin, J.A. Martens, I.F.J. Vankelecom, Polymer supported ZIF-8 membranes prepared via an interfacial synthesis method, Chem. Commun. 51 (2015) 918–920.

[92] X. Liu, N.K. Demir, Z. Wu, K. Li, Highly Water-Stable Zirconium Metal-Organic Framework UiO-66 Membranes Supported on Alumina Hollow Fibers for Desalination, J. Am. Chem. Soc. 137 (2015) 6999–7002.

Chapter 2

Fabrication of new composite membrane filled with UiO-66 nanoparticles and its application to nanofiltration

2.1. Introduction

The shortage of fresh water is one of the biggest global problems [1], which arises from the combination of population growth, industrialization, urbanization and climate change. In order to address this challenge, innovation in a wide spectrum of water treatment technologies is inevitable, in which the development of novel membrane materials plays an important role [2,3]. Since the invention of fully cross-linked polyamide thin film composites (TFC), the development of polymeric membranes has achieved tremendous applications [4,5], while rational efforts must be continuously devoted to find out a new class of membrane materials [4]. Recently, the utilization of new classes of materials with well-defined and/or oriented pores/channels has become increasingly important in separation technologies [6]. For instance, oriented nanochannels such as carbon and metal hydroxide nanotubes that are vertically embedded in support matrices led to significantly high permeation flux of water in ultra/nano filtration [7–9]. It was reported that peptide-appended pillar[5]arene channels with the inner pore diameter of 5 Å possess water permeability comparable to that of carbon nanotubes. Further, these channels are readily self-assembled into 2D-arrays suitable for membrane purposes [10,11]. A self-standing graphene oxide laminate membrane allowed extremely selective permeation toward water vapor. The gallery space of stacking graphene oxide sheets offered ideal capillary for water transport [12]. Thus, permeation and rejection through well-defined (and oriented) pores/channels at an angstrom dimension are a key for next-generation membranes.

Metal-organic frameworks (MOFs) sound appealing for membrane materials due to their exceptionally large porosity, easily tunable pore size and structural diversity [13–16]. A few pioneer researches have been reported for the use of MOFs for water filtration. Li *et al.* fabricated a nanofiltration membrane based on ZIF-8 by an interfacial method [17]. A

continuous thin selective layer (*ca.* 1-μm thick) was formed on top of a polyethersulfone (PES) support membrane. The presence of a ZIF-8 thin layer significantly enhanced the rose bengal rejection of the membrane (from 38.2% for the pristine PES to 98.9%). A deterioration of the permeability was attributed to the hydrophobic pore of ZIF-8. Sotto *et al.* utilized an MOF in a different way. They prepared a composite membrane based on a phase inversion method using PES solution that suspended Co-MOF-74 particles [18]. The MOF particles modulated the pore structure of the formed PES membrane and were also incorporated in the PES matrix as a filler. The membrane showed enhanced Bovine serum albumin rejection without sacrificing the permeation flux. Liu *et al.* deposited UiO-66 nanoparticles on the outer surface of an alumina hollow fiber. Improved salt rejection was reported at good permeability in water desalination [19]. These works pioneered promising utilization of MOFs in conjunction with a support membrane for water filtration.

In general, the morphology of a thin film composite membrane is designed to exploit the sieving ability of a selective layer without sacrificing the permeability and the mechanical robustness. Among crystalline microporous materials, zeolites are the most studied ones for the development of thin film composite membranes [20]. A major challenge has been addressed at the fabrication of a thin film overlayer in a defect-/pinhole-free manner, which copes with a tradeoff between the perfectness and the thickness of a thin film, *i.e.* between the rejection and the permeability. Several methods have been proposed such as repetitive hydrothermal synthesis of zeolite on top of a metal support membrane, crystallization of a gel as a zeolite precursor after being casted on a support membrane, and so on. Piera *et al.* proposed an alternative strategy to prepare a composite membrane with a different morphology, in which a precursor gel was filled in the porosity of a support membrane and subsequently converted into crystals to form ZSM-5 inside

porous structure of alumina [21]. Thus prepared membrane was found to be more robust against thermal expansion compared with the conventional thin film morphology. Further, the strategy is practically interesting to alleviate the necessity of a defect-free thin film over a large area.

In this chapter, a new type of a MOF/polymer composite membrane was fabricated by filling the pore of a hydrophilic regenerated cellulose support membrane with UiO-66 nanoparticles. The filled UiO-66 nanoparticles formed selective pathways for ultra/nanofiltration, while guaranteed the flexibility of the membrane. UiO-66, an MOF in Zr-based MOF family, is one of two MOFs with 12 coordination bonds between $Zr_6O_4(OH)_4$ cores and terephthalic acid linkers. It offers exceptional thermal and chemical stabilities, especially in water [22–25]. The hydrophilic pore of UiO-66 is suitable for water filtration, while its aperture size (6 Å) is sufficient to interfere with hydrated ions. Owing to these properties, UiO-66 is regarded as a potential material for water filtration membranes. The fabricated composite membrane exhibited excellent methylene blue (MB) rejection at extremely high permeability compared with commercially available membranes. The membrane also revealed consistent performance against reuse, storage in water and mechanical bending.

2.2. Experimental

2.2.1. Materials

Zirconium tetrachloride ($ZrCl_4$) (purity > 99.9%) and terephthalic acid (purity > 99%) were purchased from Sigma-Aldrich. N,N-Dimethylformamide (DMF) as a solvent was purchased from Wako Chemical Industries Ltd. These chemicals were utilized for UiO-66 preparation. A regenerated cellulose (RC) membrane (RC58, diam. 47 mm, pore size 0.2

μm, Whatman) was utilized as a support membrane. Poreless TiO_2 nanoparticles with a diameter of 30-50 nm (TTO-55A, Ishihara Sangyo Kaisha, Ltd.) were used to prepare a TiO_2/polymer composite membrane as a reference. MB (purity > 98.5%, Kanto Chemical Co., Inc) was used as a solute for filtration experiments. Polyethylene glycol (PEG) with the number-average molecular weight of 600, 2000 and 20000 Da (Wako Chemical Industries Ltd) was used for molecular weight cut-off determination. Deionized water was used throughout the experiments.

2.2.2. Preparation of UiO-66 nanoparticles

Reactant solutions were prepared in inert atmosphere by dissolving 0.30 g of $ZrCl_4$ in 90 mL of DMF and 0.22 g of terephthalic acid in 90 mL of DMF. After mixing the two solutions, 0.12 or 0.18 mL of water as a modulator was added. The mixture was reacted for 24 h under stirring at 100 °C in the inert atmosphere and thereafter aged at r.t. for overnights, resulting in stable dispersion of UiO-66 nanoparticles in DMF. It is notable that the addition of water was important to control the reaction and the formation of nanoparticles, while the inert atmosphere significantly improved the synthetic reproduction by suppressing uncontrolled intrusion of water. Thus prepared UiO-66 nanoparticles in DMF were named as MOF_1 and MOF_2 for 0.12 and 0.18 mL of the water added in the synthesis, respectively.

The UiO-66 dispersion was kept as synthesized in a refrigerator before the usage. Powder characterization was implemented after thoroughly washing the UiO-66 nanoparticles with DMF and methanol, followed by vacuum drying at 70 °C for 24 h. In preparing composite membranes, the as-synthesized dispersion was suction filtered on an RC membrane and thoroughly washed on the membrane by filtering sufficient volumes of methanol and water.

2.2.3. Membrane preparation

MOF/polymer composite membranes were prepared by a filtration method based on a suction filtration setup. An RC support membrane was taped on the filter holder. Suction filtration was performed at a differential pressure of 50 mbar, in which 1.0 mL of UiO-66 dispersion in DMF was dropped for six times (total 6.0 mL) using a micro pipette. The amount of the UiO-66 nanoparticles deposited on the support membrane was adjusted by diluting the original dispersion (MOF_1 or MOF_2) with a specified volume of DMF. After the last addition, the differential pressure was kept at 50 mbar for 5 min, and then it was increased and kept at 100 mbar for 5 min. Thus prepared composite membranes were washed with 20 mL of methanol and 250 mL of deionized water.

TiO_2-polymer composite membranes were prepared as follows: 10 mg of TiO_2 nanoparticles were dispersed in 100 mL of DMF under sonication for 3 h. After the centrifugation at 4000 rpm for 10 min, the supernatant was used to prepare membranes. 1.0 mL of TiO_2 dispersion in DMF was added for thirty times (total 30 mL) on an RC support membrane at the differential pressure of 50 mbar. After the last addition, the pressure was kept at 50 mbar for 5 min and at 100 mbar for another 5 min. Thus prepared membranes were similarly washed.

2.2.4. Characterization

Transmission FT-IR spectra were acquired for dried UiO-66 nanoparticles in KBr pellets by a Jasco FT/IR-6100 spectrometer in the range of 450-1800 cm^{-1}. The crystalline structure of dried nanoparticles was analyzed by X-ray diffraction (XRD, Rigaku SmartLab) using Cu Kα radiation (λ=1.54 Å) at 40 kV and 30 mA in the 2θ range of 5°−35°. Transmission electron microscopy (TEM, Hitachi H7100) at an acceleration voltage of 100

kV was used to determine the size and morphology of UiO-66 nanoparticles. The UiO-66 dispersion was diluted 100 times in methanol and casted onto a TEM grid.

Functional groups on membrane surfaces were analyzed based on attenuated total reflectance infrared spectroscopy (ATR-IR, Perkin Elmer Spectrum 100 FT-IR) in the range of 450-1800 cm^{-1} using a diamond crystal. The crystalline structure of UiO-66 after being deposited on the support membrane was similarly analyzed by XRD. The morphology of membranes was observed by scanning electron microscopy (SEM, Hitachi S-4100) at an accelerated voltage of 20 kV. For cross-sectional images, membranes were cryo-fractured into small pieces and subjected to Pt sputtering for 60 s before the measurements.

2.2.5. Filtration experiments

Filtration performance of composite membranes was evaluated by suction filtration of 100 mL of MB aqueous solution (1.0 μM) at the differential pressure of 100 mbar. It must be noted that such a low differential pressure arises from extremely high permeability of the developed membranes, as has been the case for the previously developed membranes with oriented nanochannels [8,9]. The MB concentration in the feed and permeate solutions was determined by the absorption intensity at the wavelength of 665 nm measured by a JASCO V670 spectrometer. The rejection and flux were measured at each 1-2 min, and respectively expressed by cumulative and averaged values along the filtration time.

In order to determine the molecular weight cut-off (MWCO) of composite membranes, filtration tests were performed using PEG dissolved in deionized water (0.5 ppm, 100 mL). The MWCO value is regarded as the molecular weight of PEG that can be rejected by a membrane at 90% [26–28]. PEG with three different molecular weights (600, 2000, and

20000 Da) was employed. The macromolecular diameter of PEG was estimated as 1.22, 2.28, and 7.35 nm for 600, 2000, 20000 Da, respectively, based on Eq. (1).

$$d = 0.524 \times (M_w)^{0.5} - 0.6 \qquad (2.1),$$

where d is the molecular diameter (Å) and M_w is the weight-average molecular weight (Da) [29,30]. The PEG concentration in the feed and permeate solutions was determined by spectrometric titration of the iodine complex [31,32].

The durability of composite membranes was evaluated in three ways:

i) *Reusability*: A composite membrane that was once used for the above-mentioned filtration experiment for the MB aqueous solution was extensively washed with deionized water, and subjected to the same filtration experiment. The cycle was repeated three times, in which potential deterioration in the rejection was observed.

ii) *Stability in water*: A composite membrane was immersed in deionized water for 4-30 days, followed by the filtration experiment using the MB aqueous solution.

iii) *Flexibility*: A composite membrane was bent (a typical image was shown later) before the filtration experiment.

2.2.6. Adsorption capacity of membranes

In order to understand a potential contribution of adsorption to the separation of MB, the adsorption capacity of membranes was studied. Membranes were soaked in 100 mL of MB aqueous solutions at concentrations of 1.0, 2.0, 4.0, 8.0, 12 and 16 μM at r.t. for 42 h. The amount of the adsorbed MB was evaluated from the MB concentration in the supernatant solution to plot adsorption isotherms. The equilibrium adsorption dictates the upper limit of the adsorption contribution to the MB rejection.

2.3. Results and discussion

2.3.1. Preparation and characterization

Two MOF samples were prepared by reacting $ZrCl_4$ and terephthalic acid in DMF. The size of the resultant MOF particles was controlled by the water amount. Upon heating the reaction mixture, it took 10 h and 8 h for the formation of MOF_1 and MOF_2 to be visible, respectively. The yields (after washing) were derived as 24.3% and 34.3% respectively for MOF_1 and MOF_2. Thus, it is clear that water promoted the MOF formation, while the relatively low yields came from the limited amount of water added to control the particle size.

Fig. 2.1a shows the IR spectra of dried UiO-66 nanoparticles (MOF_1 and MOF_2) in the skeletal mode region. The spectra exhibit typical peaks of UiO-66 reported in literature [24,33,34]: An intense doublet at 1574 and 1395 cm^{-1} for the in- and out-of-phase stretching modes of the carboxylate group, and bands at 475, 744 and 548 cm^{-1} for the bending of OH and CH mixed with Zr−O modes, and Zr-(OC) asymmetric stretching vibration, respectively. XRD patterns of dried UiO-66 nanoparticles (Fig. 2.1b) also show consistent results: 7.26, 8.39, 11.93, and 14.64° of 2θ corresponding to the (111), (002), (022), and (222) planes of the face-centered cubic crystal of UiO-66 [19,23,24,35]. TEM images show that synthesized MOF_1 particles had polygonal shapes, and the mean diameter was approximately 10 nm with a relatively broad distribution (Fig. 2.1c). Meanwhile, MOF_2 consisted of cubic particles with the dimension about 55 nm (Fig. 2.1d). The difference of the particle morphology between MOF_1 and MOF_2 indicated that the water amount in the reaction solution clearly affected the nanoparticle formation [36–38]. Water as a modulator enhances the nucleation rate to form homogeneous crystals, while

suppresses the precipitation of amorphous products [36,38]. In fact, the synthesis without the water addition led to an uncontrollable particle size distribution of UiO-66.

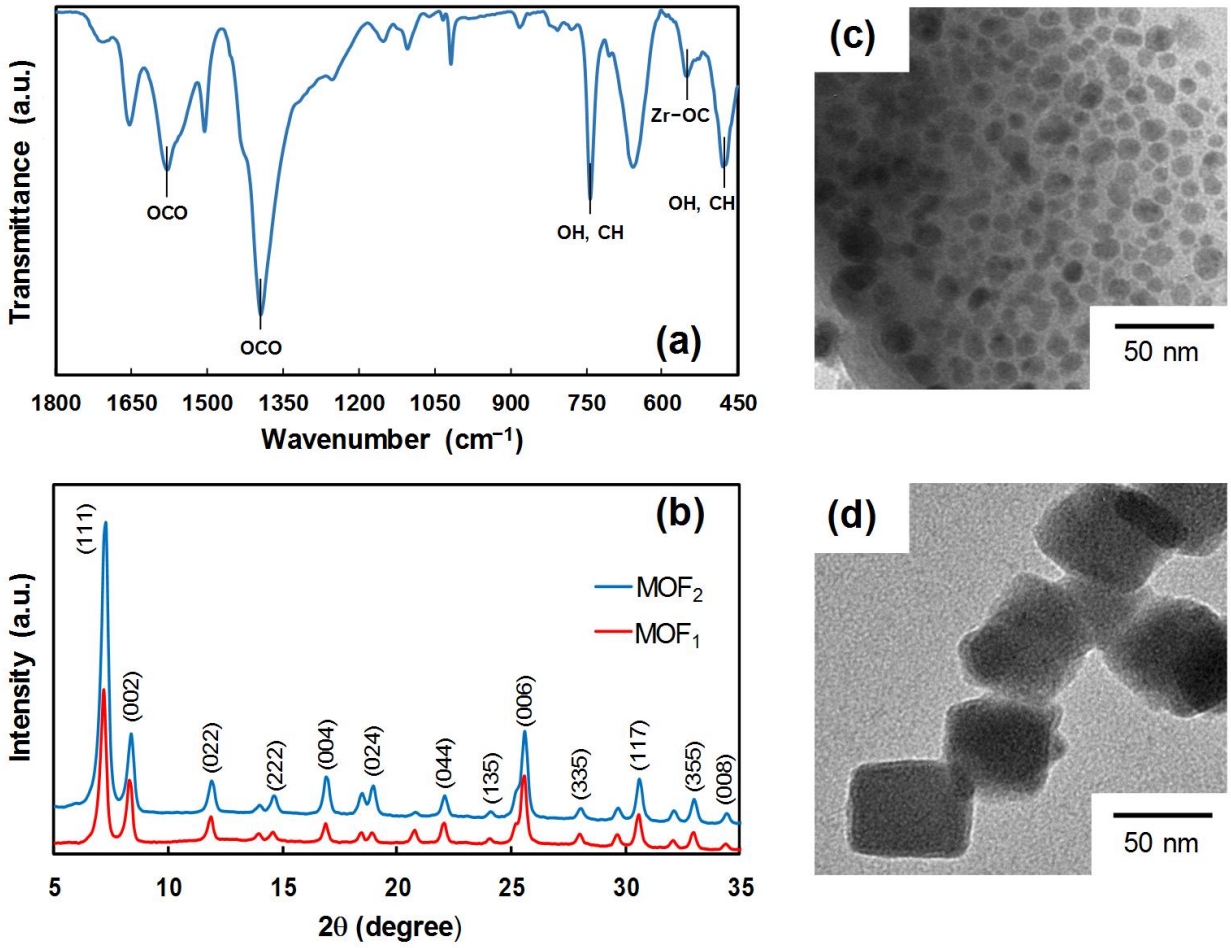

Fig. 2.1. Characterization of UiO-66 nanoparticles: a) FT-IR spectrum, b) XRD patterns, and c,d) TEM images of MOF_1 and MOF_2, respectively

Three kinds of MOF-polymer composite membranes were prepared using the above-synthesized UiO-66 dispersion (Table 2.1), and subsequently characterized by XRD, ATR-IR, and SEM (Fig. 2.2). In XRD (Fig. 2.2a), it can be seen that the diffraction peaks relevant to UiO-66 were superimposed on those for the RC membrane. A greater contribution of UiO-66 crystals with respect to the RC membrane diffraction was identified for M_{MOF2} than for M_{MOF1}-1. In ATR-IR spectra (Fig. 2.2b), the superposition of the UiO-66 absorption

bands with those of the support [39,40] was again observed for M_{MOF2}. In contrast, the spectrum of M_{MOF1}-1 showed the total absence of the absorption bands from UiO-66. The observed differences between M_{MOF1}-1 and M_{MOF2} in XRD and ATR-IR were clarified by SEM images (Fig. 2.2d,e). The RC membrane exhibited a highly porous morphology with a large number of cellulose fibers disorderly interlaced among each other. SEM images of the composite membranes showed completely different morphologies between M_{MOF1} and M_{MOF2}. MOF_2 formed a thin layer of UiO-66 nanoparticles stacked on the support membrane. The thickness was estimated as *ca.* 2 µm. Conversely, few UiO-66 nanoparticles were observed in the top view of M_{MOF1}-1, as they were mainly captured inside the pore network of the support membrane. This discrepancy was due to the difference in the particle size: The pores of the RC membrane were quickly plugged by the larger MOF_2 nanoparticles, leading to the formation of a thin layer. The smaller MOF_1 nanoparticles deeply penetrated in the RC membrane, being entrapped in the pores. We could not observe any of MOF_1 nanoparticles which went through the RC membrane into the permeate side during the preparation and filtration experiments. This fact suggested strong adhesion of the nanoparticles to the pore wall of the RC membrane.

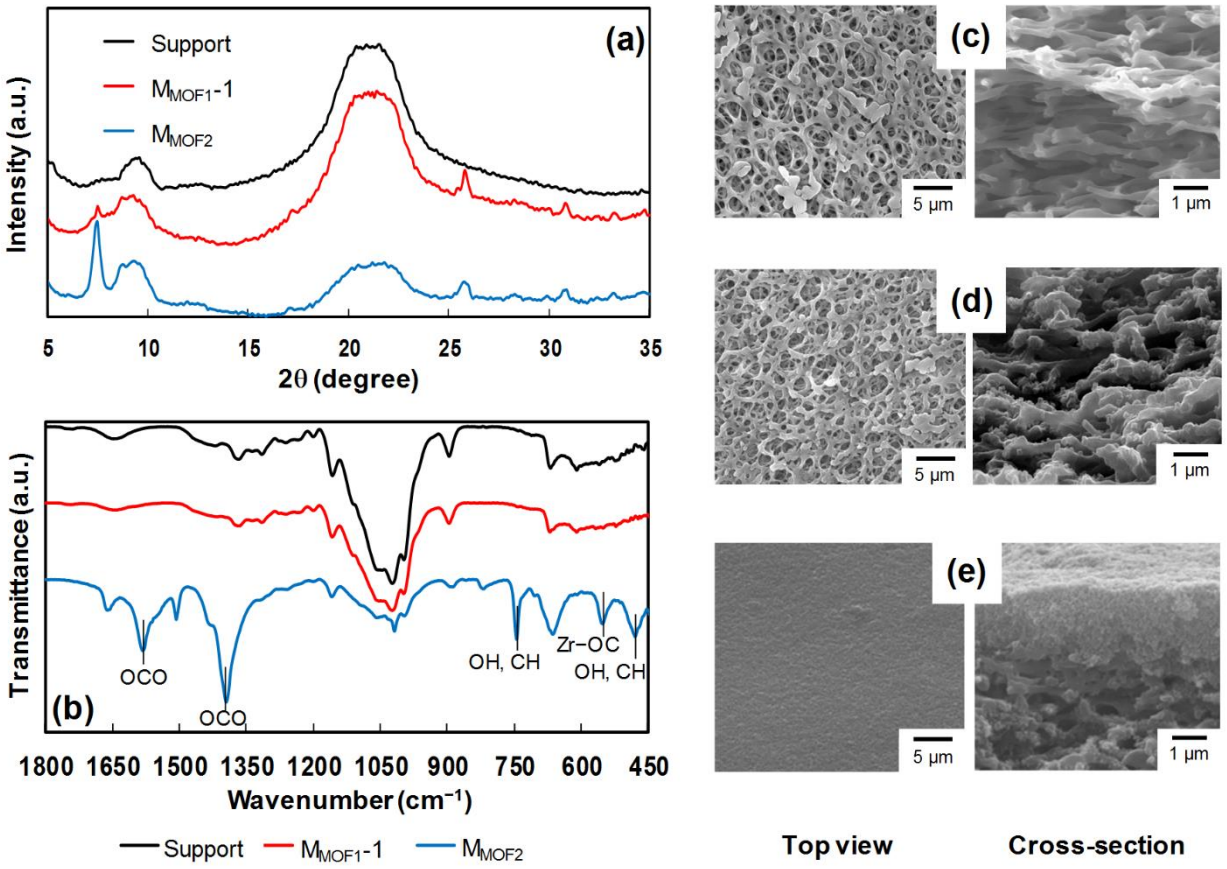

Fig. 2.2. Characterization of the support and composite membranes: a) XRD patterns, b) ATR-IR spectra, c–e) SEM images both in top and cross-sectional views of support, M_{MOF1}-1, M_{MOF2} membranes, respectively.

It is notable that in the case of as-synthesized UiO-66 nanoparticles, well-defined crystals (Fig. 2.1b) were only obtained when the sample was soaked in methanol for three days to fully remove residual molecules remaining inside the MOF structure [41–43]. On the other hand, UiO-66 nanoparticles deposited on an RC membrane formed similarly well-defined crystals by washing through suction filtration for several minutes (Fig. 2.2a). Namely, the suction filtration enabled efficient washing of residual molecules. It was likely that solvent molecules might permeate through the intraparticle channels of UiO-66.

2.3.2. Filtration performance

Employing the prepared composite and support membranes, filtration tests were performed for MB aqueous solution. Typical results of these experiments are shown in Fig. 2.3a. The RC membrane exhibited the highest permeability, completing 100 mL filtration within 4 min. The pore size of the RC membrane (0.2 μm) is much larger than the molecular size of MB. However, the MB rejection was 100% for the initial 50 mL permeate, followed by a significant drop of the rejection in the later stage. This was mainly due to the MB adsorption on cellulose and its saturation beyond the adsorption capacity (examined later). The inclusion of UiO-66 nanoparticles in the pore of the RC membrane (M_{MOF1}) led to the elongation of the filtration time from 4 to 7.5 min and the full retention of the perfect rejection for 100 mL. The permeability value was calculated as 7860 ± 374 L/m^2·h·bar, which was 30-500 times greater than those for commercially available ultra/nano filtration membranes: e.g. 100-300 L/m^2·h·bar for PVDF ultrafiltration membranes [44] and 15 L/m^2·h·bar for UTC-20 nanofiltration membranes from Toray Industries, Inc. [45]. This extremely high permeability of M_{MOF1} seems to arise from the combination of the filled morphology and the mechanism of the selective permeation. The latter will be further discussed later.

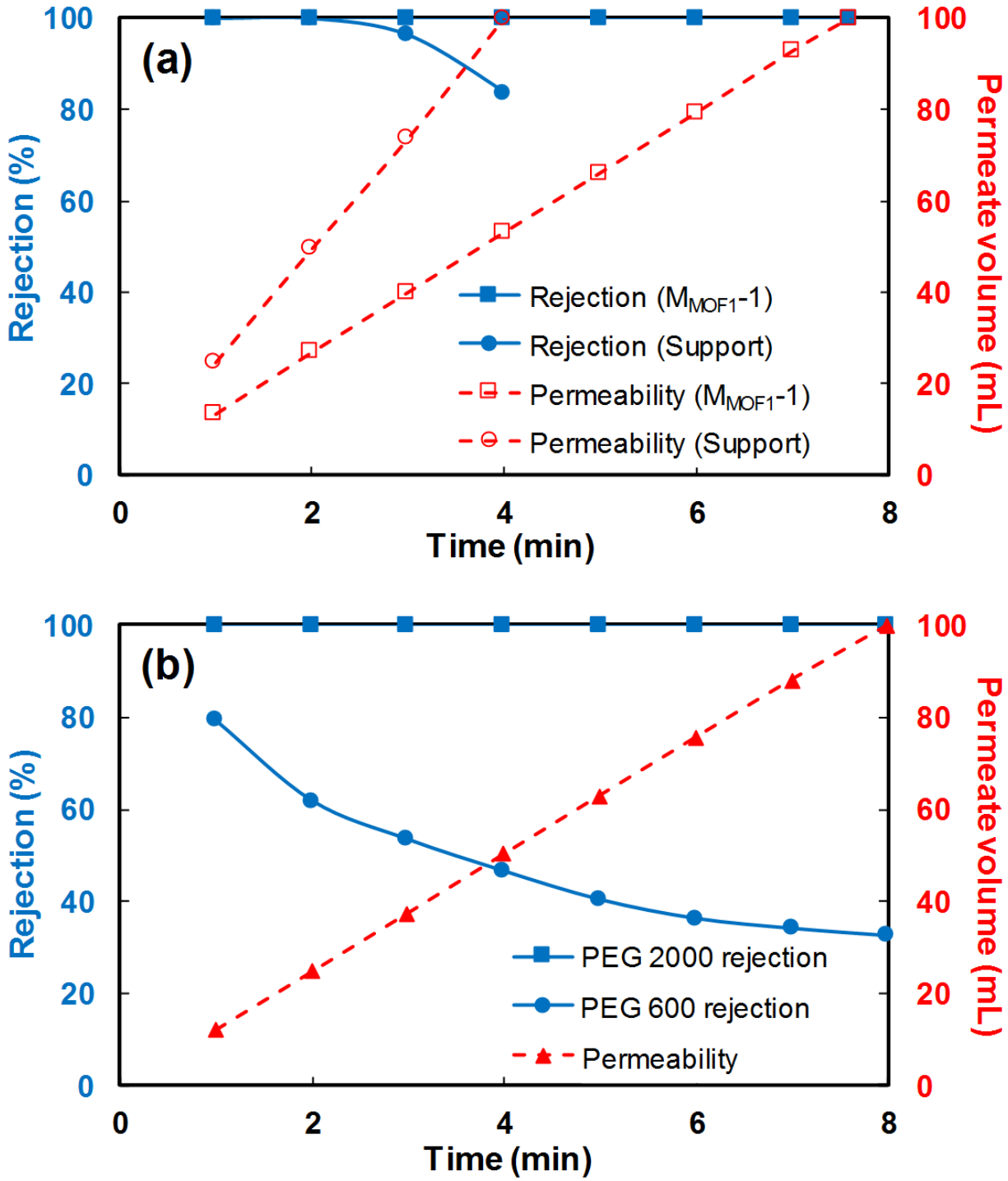

Fig. 2.3. Filtration performance: a) MB filtration using the RC and M_{MOF1}-1 membranes, b) filtration of PEG with different molecular weights using the M_{MOF1}-1 membrane

The performance of the membranes is thus obtained and summarized in Table 2.1. The experiments were performed at least twice for each same type of membranes that were

prepared independently under the same condition so as to obtain error ranges (lower than 5% for the flux and 0.1% for the rejection). The flux of the RC membrane was the highest with poor rejection at 83.7 ± 0.1%. All of the composite membranes showed improved rejection in cost of the flux. However, the tradeoff between the flux and rejection largely depended on the particle size of UiO-66. Even with the same dilution ratio, the performance of M_{MOF2} was inferior to that of M_{MOF1}-1 in both the flux and rejection. When the deposition amount of MOF_1 nanoparticles was reduced into half (M_{MOF1}-2), the rejection was slightly deteriorated with a partial recovery of the permeability.

Table 2.1. List of prepared MOF-polymer composite membranes and their performance in filtration of MB aqueous solution

Membrane	UiO-66 solution[a] MOF_1 (mL)	UiO-66 solution[a] MOF_2 (mL)	DMF[a] (mL)	Flux ($L/m^2 \cdot h$)[b]	Rejection (%)[b]
RC	0	0	0	1733.8 ± 31.2	83.7 ± 0.1
M_{MOF1}-1	3	0	3	785.8 ± 37.4	100
M_{MOF1}-2	1.5	0	4.5	1041.6 ± 43.6	98.9 ± 0.1
M_{MOF2}	0	3	3	461.5 ± 18.7	95.0 ± 0.1

[a] A stock solution of UiO-66 in DMF was diluted by a specified volume of DMF and used for membrane preparation. In total, 6.0 mL of a diluted solution was suction filtered on an RC membrane.

[b] The performance of a membrane was tested by suction filtration of MB aqueous solution (1.0 μmol, 100 mL) at the differential pressure of 100 mbar. The flux was determined by permeate volume after every one minute. The rejection was determined by equation $R(\%) = \frac{C_0 - C_p}{C_0} \times 100\%$, where C_0 and C_p are the solute concentrations in the feed and permeate, respectively. The experiments were repeated for at least two membranes ($N \geq 2$) that were prepared under the same condition.

It became clear that the deposition of UiO-66 nanoparticles significantly improved the rejection, keeping relatively high permeability. However, its mechanism was unclear: The molecular size of MB is greater than the intraparticle channel of UiO-66. On the other hand, it was reported that MB can adsorb on the outermost surfaces of UiO-66 (not in the channel) [46]. Hereafter, a series of experiments were implemented to identify the origin of the

improved rejection, where M_{MOF1}-1 bearing the best performance was employed as a representative.

2.3.3. Adsorption experiment

The adsorption capacity of the support and M_{MOF1}-1 membranes for MB is compared in Fig. 2.4. A linear increment in the adsorption amount was observed along the MB concentration for both of the membranes, which corresponded to almost 100% entrapment of MB. The linear increment continued over the experimental range for the support membrane, while the saturation was reached for the composite membrane. The adsorption capacity of the M_{MOF1}-1 was derived as 1.75 μg/mg, while the capacity of the support was greater than >3.32 μg/mg. In a separate experiment, the adsorption capacity of the MOF_1 nanoparticles was measured as 2.8 mg/g. Considering that 1.89 mg of MOF_1 was deposited on a support membrane of the total weight of 33.16 mg, it is clear that the adsorption of MB on the outermost surfaces of UiO-66 was negligible. Rather, it seemed that the interaction of UiO-66 with cellulose and/or pore plugging by the inclusion of the nanoparticles significantly reduced the adsorption capacity of the composite membrane. These results strongly indicated that the improved rejection came from the molecular sieving mechanism, not from the adsorption mechanism.

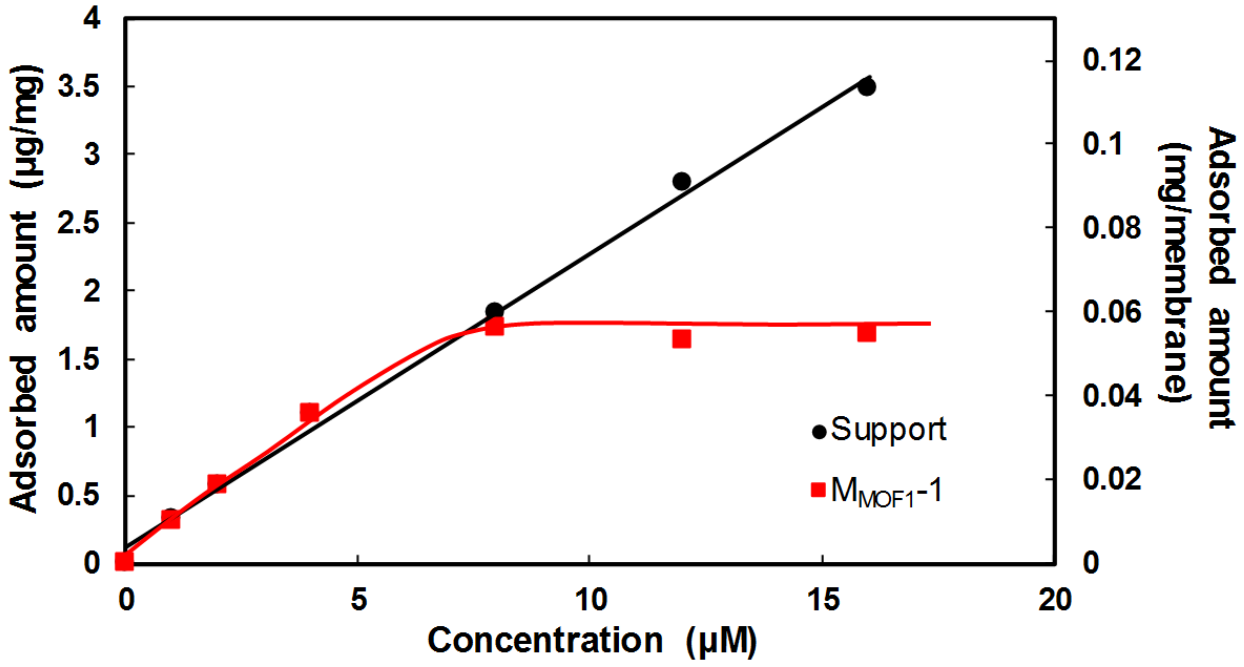

Fig. 2.4. Adsorption isotherm of MB for the RC and M_{MOF1}-1 membranes

2.3.4. PEG filtration

In order to reach a closer insight into the rejection mechanism, the MWCO of the composite membrane (M_{MOF1}-1) was investigated based on the filtration of PEG 600, 2000 and 20000 (Da). The filtration results are summarized in Fig. 3 and Table 2.2. It was found that the composite membrane was able to completely reject PEG 2000 with the molecular size of 2.28 nm. The rejection became as poor as 35% for PEG 600 with the diameter of 1.22 nm. Such a sudden drop from 100% rejection clarified the presence of a well-defined MWCO between 1.22 to 2.28 nm. Furthermore, the adsorption of PEG on the composite membrane was not plausible, as the monotonous rejection drop for PEG 600 indicated negligible adsorption capacity (Fig. 2.3b). In accordance with the adsorption experiment, the molecular sieving by UiO-66 nanoparticles was again supported as a plausible cause of the improved rejection of MB, whose molecular size is 1.5-1.6 nm [47,48].

Table 2.2. PEG filtration using the composite membrane (M_{MOF1}-1)

Molecular weight of PEG (Da)	Molecular size (nm)[a]	Flux (L/m^2·h)[b]	Rejection (%)[b]
20000	7.35	879.4 ± 18.7	100
2000	2.28	829.5 ± 16.8	100
600	1.22	779.6 ± 12.4	34.9 ± 1.3

[a] The molecular size was estimated according to Eq. (1).
[b] Suction filtration of PEG aqueous solution (0.5 ppm, 100 mL) was conducted twice at the differential pressure of 100 mbar.

Here, the origin of the molecular sieving by UiO-66 nanoparticles is discussed: Rejection could arise either from the intraparticle channel of the MOF crystal or from interparticle voids among filled UiO-66 nanoparticles. With the assumption of the closest packing, the dimension of the interparticle voids could be estimated as 3.1 nm for the particle size around 10 nm for MOF_1. When the packing deviates from the ideal closest packing, the void dimension must become greater and distributed. Considering the observed sharp cut-off in 1.22-2.28 nm, neither the estimated void dimension nor its distribution are reasonable. Thus, it was believed that the improved MB rejection dominantly came from the intraparticle channel of the MOF crystal. A slight inconsistency in the dimension between 0.6 nm of the pore aperture of UiO-66 and 1.22-2.28 nm of MWCO might be explained by an elongation of PEG 600 oligomers inside the pore channel along the flow direction [49]. In Table 2.1, the MB rejection for M_{MOF2} and M_{MOF1}-2 was slightly lower than that of M_{MOF1}-1. This rejection failure was plausibly attributed to the leakage from interparticle voids (since the intraparticle channel is always the same).

2.3.5. TiO_2-polymer composite membranes

In order to further identify the rejection mechanism, a filtration experiment of MB aqueous solution was conducted using a TiO_2-polymer composite membrane.

Poreless TiO_2 nanoparticles deposited on an RC membrane could offer interparticle void-based filtration. The suction filtration of TiO_2 dispersion in DMF led to the formation of a thin film layer with the thickness of *ca.* 0.6 μm (Fig. 2.5). The filtration test using 100 mL of MB aqueous solution (1.0 μM) led to 723.5 ± 18.7 $L/m^2 \cdot h$ in the flux and 77.36 ± 0.95% in the rejection. Thus, poreless TiO_2 offered only interparticle voids for water transport, leading to poor rejection as well as relatively high flux. It is reasonable that interparticle voids between 30-50 nm particles never contributed to the MB rejection. Rather, TiO_2 nanoparticles blocked the adsorption sites of the RC membrane to deteriorate the rejection.

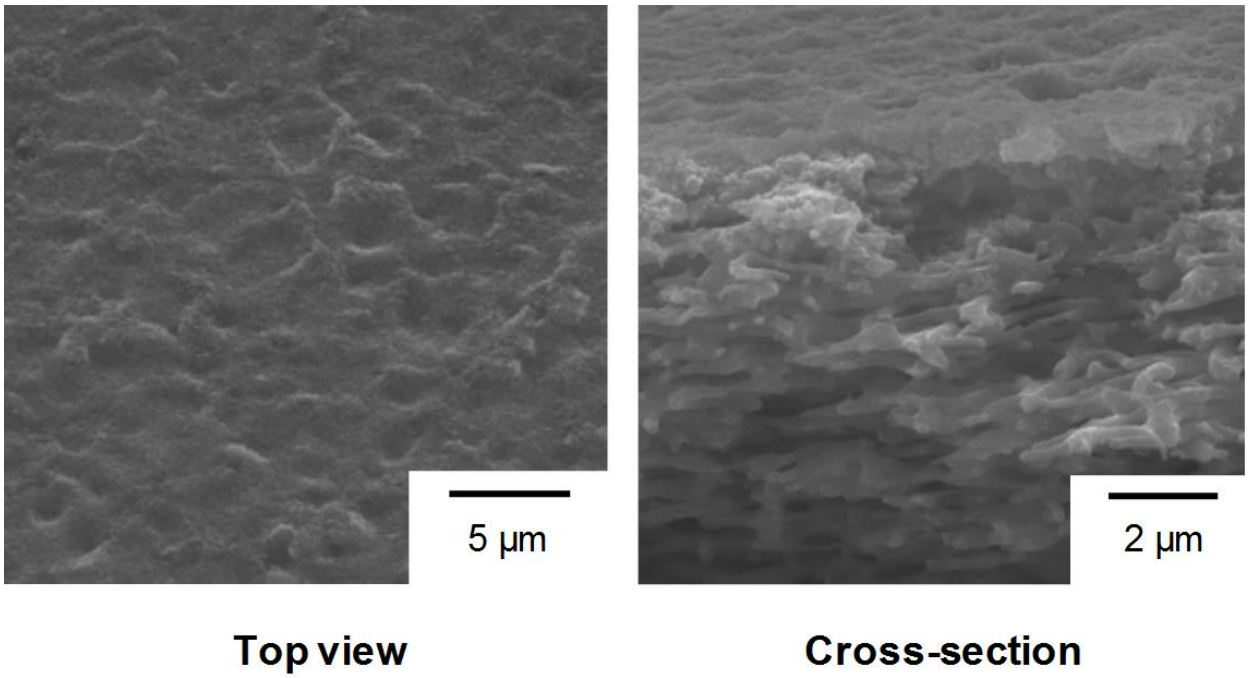

Fig. 2.5. SEM images of the TiO_2-RC composite membrane

2.3.6. Durability of composite membranes

The durability of the composite membrane (M_{MOF1}-1) with a filled morphology was investigated in terms of reusability, stability in water, and flexibility upon bending. Fig. 2.6 summarizes the results of membrane performance for the filtration of 100 mL of MB

aqueous solution. The reuse of the composite membrane unchanged both the flux and rejection of the membrane for at least three times (Fig. 2.6a). This result indicated that UiO-66 nanoparticles were well immobilized inside the support membrane, and the intraparticle channels were free from the adsorption of MB. The membrane performance was well retained even after the membrane was soaked in deionized water for one month due to the structural stability of UiO-66 (Fig. 2.6b). Moreover, the composite membrane showed consistent performance even after being bent by forceps, which demonstrated a potential benefit of the morphology of the developed composite membrane (Fig. 2.6c,d) for advanced modules such as spiral-wound and hollow tube filters.

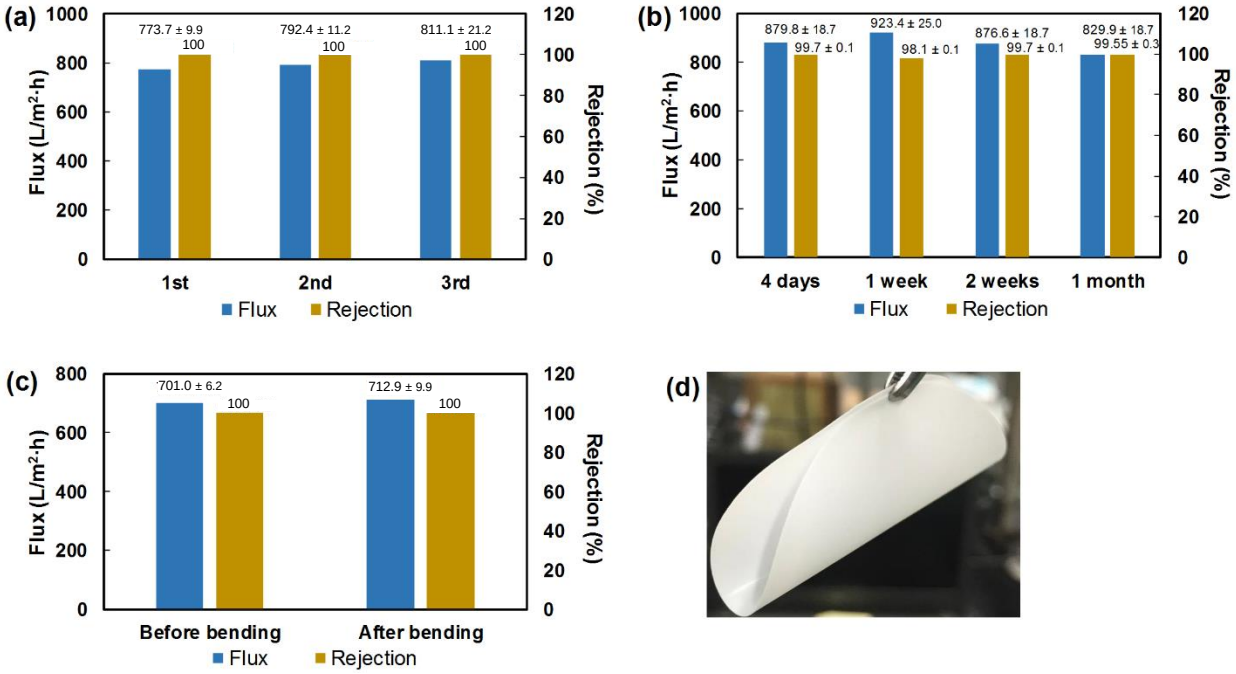

Fig. 2.6. Durability of the M_{MOF1}-1 membrane tested in MB filtration: a) When reused, b) when stored in water, and c,d) when bent

2.4. Conclusions

Novel composite membranes were prepared by filling the porosity of a regenerated cellulose membrane by UiO-66 nanoparticles. UiO-66 nanoparticles with the average size

of 50 nm formed a thin selective layer on the support, while nanoparticles with the size of 10 nm were filled in the porosity of the support to create a selective pathway. Both of the membranes significantly improved the rejection of methylene blue, but the filled morphology was superior in terms of the permeability and rejection. A set of experiments proved that the rejection of the composite membrane was based on a molecular sieving mechanism. The molecular weight cut-off of the membrane was determined within 1.22-2.28 nm based on the filtration of polyethylene glycol. The composite membrane exhibited excellent durability against repetitive filtration, storage in water for one month, and mechanical bending.

In this chapter, I revealed promising aspects of MOF nanoparticle-filled composite membranes in water nanofiltration. On the other hand, the rejection of small ions may require more perfect packing, which is addressed in chapter 4.

2.5. References

[1] M. Shannon, P.W. Bohn, M. Elimelech, J.G. Georgiadis, B.J. Mariñas, A.M. Mayes, Science and technology for water purification in the coming decades, Nature 452 (2008) 301–310.

[2] J.-Y. Lee, C.Y. Tang, F. Huo, Fabrication of porous matrix membrane (PMM) using metal-organic framework as green template for water treatment, Sci. Rep. 4 (2014) 3740.

[3] M.M. Pendergast, E.M.V. Hoek, A review of water treatment membrane nanotechnologies, Energy Environ. Sci. 4 (2011) 1946−1971.

[4] K.P. Lee, T.C. Arnot, D. Mattia, A review of reverse osmosis membrane materials for desalination-Development to date and future potential, J. Memb. Sci. 370 (2011) 1–22.

[5] J.R. Werber, C.O. Osuji, M. Elimelech, Materials for next-generation desalination and water purification membranes, Nat. Rev. Mater. 1 (2016) 16018.

[6] R.K. Joshi, P. Carbone, F.C. Wang, V.G. Kravets, Y. Su, I.V. Grigorieva, H. A. Wu, A.K. Geim, R.R. Nair, Precise and Ultrafast Molecular Sieving Through Graphene Oxide Membranes, Science 343 (2014) 752–754.

[7] J.H. Walther, K. Ritos, E.R. Cruz-Chu, C.M. Megaridis, P. Koumoutsakos, Barriers to superfast water transport in carbon nanotube membranes, Nano Lett. 13 (2013) 1910–1914.

[8] H. Huang, Z. Song, N. Wei, L. Shi, Y. Mao, Y. Ying, L. Sun, Z. Xu, X. Peng, Ultrafast viscous water flow through nanostrand-channelled graphene oxide membranes, Nat. Commun. 4 (2013) 2979.

[9] X. Peng, J. Jin, Y. Nakamura, T. Ohno, I. Ichinose, Ultrafast permeation of water

through protein-based membranes, Nat. Nanotechnol. 4 (2009) 353–357.

[10] Y.-X. Shen, W. Si, M. Erbakan, K. Decker, R. De Zorzi, P.O. Saboe, Y.J. Kang, S. Majd, P.J. Butler, T. Walz, A. Aksimentiev, J. Hou, M. Kumar, Highly permeable artificial water channels that can self-assemble into two-dimensional arrays, Proc. Natl. Acad. Sci. U. S. A. 112 (2015) 9810–9815.

[11] M. Barboiu, Artificial water channels – incipient innovative developments, Chem. Commun. 52 (2016) 5657–5665.

[12] R.R. Nair, H.A. Wu, P.N. Jayaram, I.V. Grigorieva, A.K. Geim, Unimpeded Permeation of Water Through Helium-Leak-Tight Graphene-Based Membranes, Science 335 (2012) 442–444.

[13] S. Qiu, M. Xue, G. Zhu, Metal-organic framework membranes: from synthesis to separation application, Chem. Soc. Rev. 43 (2014) 6116–6140.

[14] N. Yanai, S. Granick, Directional self-assembly of a colloidal metal-organic framework, Angew. Chemie. Int. Ed. 51 (2012) 5638–5641.

[15] H.-C. "Joe" Zhou, S. Kitagawa, Metal–Organic Frameworks (MOFs), Chem. Soc. Rev. 43 (2014) 5415–5418.

[16] W. Lu, Z. Wei, Z.-Y. Gu, T.-F. Liu, J. Park, J. Park, J. Tian, M. Zhang, Q. Zhang, T. Gentle III, M. Bosch, H.-C. Zhou, Tuning the structure and function of metal–organic frameworks via linker design, Chem. Soc. Rev. 43 (2014) 5561–5593.

[17] Y. Li, L.H. Wee, A. Volodin, J. a Martens, I.F.J. Vankelecom, Polymer supported ZIF-8 membranes prepared via an interfacial synthesis method, Chem. Commun. 51 (2015) 918–920.

[18] A. Sotto, G. Orcajo, J.M. Arsuaga, G. Calleja, J. L.-Aguirre, Preparation and characterization of MOF-PES ultrafiltration membranes, J. Appl. Polym. Sci. 132

(2015) 41633.

[19] X. Liu, N.K. Demir, Z. Wu, K. Li, Highly Water-Stable Zirconium Metal-Organic Framework UiO-66 Membranes Supported on Alumina Hollow Fibers for Desalination, J. Am. Chem. Soc. 137 (2015) 6999–7002.

[20] N. Rangnekar, N. Mittal, B. Elyassi, J. Caro, M. Tsapatsis, Zeolite membranes − a review and comparison with MOFs, Chem. Soc. Rev. 44 (2015) 7128–7154.

[21] E. Piera, A. Giroir-Fendler, J.A. Dalmon, H. Moueddeb, J. Coronas, M. Menéndez, J. Santamaría, Separation of alcohols and alcohols/O_2 mixtures using zeolite MFI membranes, J. Memb. Sci. 142 (1998) 97–109.

[22] N.C. Burtch, H. Jasuja, K.S. Walton, Water Stability and Adsorption in Metal − Organic Frameworks, Chem. Rev. 114 (2014) 10575−10612.

[23] J.H. Cavka, S. Jakobsen, U. Olsbye, N. Guillou, C. Lamberti, S. Bordiga, K.P. Lillerud, A New Zirconium Inorganic Building Brick Forming Metal Organic Frameworks with Exceptional Stability, J. Am. Chem. Soc. 130 (2008) 13850–13851.

[24] L. Valenzano, B. Civalleri, S. Chavan, S. Bordiga, M.H. Nilsen, S. Jakobsen, K.P. Lillerud, C. Lamberti, Disclosing the complex structure of UiO-66 metal organic framework: A synergic combination of experiment and theory, Chem. Mater. 23 (2011) 1700–1718.

[25] F. Ragon, B. Campo, Q. Yang, C. Martineau, A.D. Wiersum, A. Lago, V. Guillerm, C. Hemsley, J.F. Eubank, M. Vishnuvarthan, F. Taulelle, P. Horcajada, A. Vimont, P.L. Llewellyn, M. Daturi, S. Devautour-Vinot, G. Maurin, C. Serre, T. Devic, G. Clet, Acid-functionalized UiO-66(Zr) MOFs and their evolution after intra-framework cross-linking: structural features and sorption properties, J. Mater. Chem. A. 3 (2015) 3294–3309.

[26] T. Tsuru, S. Izumi, T. Yoshioka, M. Asaeda, Temperature effect on transport performance by inorganic nanofiltration membranes, AIChE J. 46 (2000) 565–574.

[27] T. Tsuru, M. Miyawaki, H. Kondo, T. Yoshioka, M. Asaeda, Inorganic porous membranes for nanofiltration of nonaqueous solutions, Sep. Purif. Technol. 32 (2003) 105–109.

[28] Q. Chen, P. Yu, W. Huang, S. Yu, M. Liu, C. Gao, High-flux composite hollow fiber nanofiltration membranes fabricated through layer-by-layer deposition of oppositely charged crosslinked polyelectrolytes for dye removal, J. Memb. Sci. 492 (2015) 312–321.

[29] X. Chen, W. Zhang, Y. Lin, Y. Cai, M. Qiu, Y. Fan, Preparation of high-flux ɣ-alumina nanofiltration membranes by using a modified sol-gel method, Microporous Mesoporous Mater. 214 (2015) 195–203.

[30] P. Puhlfürß, A. Voigt, R. Weber, M. Morbé, Microporous TiO_2 membranes with a cut off <500 Da, J. Memb. Sci. 174 (2000) 123–133.

[31] A. Sabde, M. Trivedi, V. Ramachandhran, M.S. Hanra, B.M. Misra, Casting and characterization of cellulose acetate butyrate based UF membranes, Desalination 114 (1997) 223–232.

[32] Y. Lv, H.C. Yang, H.Q. Liang, L.S. Wan, Z.K. Xu, Novel nanofiltration membrane with ultrathin zirconia film as selective layer, J. Memb. Sci. 500 (2016) 265–271.

[33] J.B. DeCoste, G.W. Peterson, B.J. Schindler, K.L. Killops, M. A. Browe, J.J. Mahle, The effect of water adsorption on the structure of the carboxylate containing metal–organic frameworks Cu-BTC, Mg-MOF-74, and UiO-66, J. Mater. Chem. A. 1 (2013) 11922−11932.

[34] J.B. DeCoste, G.W. Peterson, H. Jasuja, T.G. Glover, Y. Huang, K.S. Walton,

Stability and degradation mechanisms of metal-organic frameworks containing the $Zr_6O_4(OH)_4$ secondary building unit, J. Mater. Chem. A. 1 (2013) 5642–5650.

[35] M. Kandiah, S. Usseglio, S. Svelle, U. Olsbye, K.P. Lillerud, M. Tilset, Post-synthetic modification of the metal–organic framework compound UiO-66, J. Mater. Chem. 20 (2010) 9848−9851.

[36] Z. Hu, D. Zhao, De facto methodologies toward the synthesis and scale-up production of UiO-66-type metal–organic frameworks and membrane materials, Dalton Trans. 44 (2015) 19018–19040.

[37] Y. Bai, Y. Dou, L.H. Xie, W. Rutledge, J.R. Li, H.C. Zhou, Zr-based metal–organic frameworks: design, synthesis, structure, and applications, Chem. Soc. Rev. 45 (2016) 2327−2367.

[38] B. Bueken, H. Reinsch, N. Reimer, I. Stassen, F. Vermoortele, R. Ameloot, N. Stock, C.E.A. Kirschhock, D. De Vos, A zirconium squarate metal–organic framework with modulator-dependent molecular sieving properties, Chem. Commun. 50 (2014) 10055–10058.

[39] M. Tsuboi, Infrared spectrum and crystal structure of cellulose, J. Polym. Sci. 25 (1957) 159–171.

[40] M. Fan, D. Dai, B. Huang, Fourier Transform Infrared Spectroscopy for natural fibres, Salih, S.M. (Ed.), Fourier Transform - Materials Analysis, InTech: Rijeka, Croatia, 2012; pp. 45–68.

[41] X. Zhu, J. Gu, Y. Wang, B. Li, Y. Li, W. Zhao, J. Shi, Inherent anchorages in UiO-66 nanoparticles for efficient capture of alendronate and its mediated release, Chem. Commun. 50 (2014) 8779–8782.

[42] G.E. Cmarik, M. Kim, S.M. Cohen, K.S. Walton, Tuning the adsorption properties

of uio-66 via ligand functionalization, Langmuir 28 (2012) 15606–15613.

[43] G. Lu, C. Cui, W. Zhang, Y. Liu, F. Huo, Synthesis and self-assembly of monodispersed metal-organic framework microcrystals, Chem. Asian J. 8 (2013) 69–72.

[44] M.S. Araki, C.M. Coutinho, L.A.G. Gonçalves, L.A. Viotto, Solvent permeability in commercial ultrafiltration polymeric membranes and evaluation of the structural and chemical stability towards hexane, Sep. Purif. Technol. 71 (2010) 13–21.

[45] B.V.D. Bruggen, C. Vandecasteele, Flux decline during nanofiltration of organic components in aqueous solution, Environ. Sci. Technol. 35 (2001) 3535–3540.

[46] Q. Chen, Q. He, M. Lv, Y. Xu, H. Yang, X. Liu, F. Wei, Selective adsorption of cationic dyes by UiO-66-NH_2, Appl. Surf. Sci. 327 (2015) 77–85.

[47] X. Shao, W. Lu, R. Zhang, F. Pan, Enhanced photocatalytic activity of TiO_2-C hybrid aerogels for methylene blue degradation, Sci. Rep. 3 (2013) 3018.

[48] X. Zhao, X. Bu, T. Wu, S.-T. Zheng, L. Wang, P. Feng, Selective anion exchange with nanogated isoreticular positive metal-organic frameworks, Nat. Commun. 4 (2013) 2344.

[49] H. Bai, Y. Zhou, X. Wang, L. Zhang, The permeability and mechanical properties of cellulose acetate membranes blended with polyethylene glycol 600 for treatment of municipal sewage, Procedia Environ. Sci. 16 (2012) 346–351.

Chapter 3

Synthesis of poly(ethylene glycol) methacrylate-grafted UiO-66 nanoparticles and application for new composite membranes

3.1. Introduction

In recent years, the dramatic increase in the release of oily waste water from various industries including oil refinery, pharmaceutical, cosmetic, food, etc. led to a risk factor for environment and human health [1-3]. Traditional technologies such as gravity separation, air flotation, coagulation and flocculation, are useful for separation of oil/water mixture. However, these technologies ineffectively separate emulsified oil/water system because of the small droplet size of microemulsion or nanoemulsions [4]. Therefore, an effective, low cost technology for separation of oil/water emulsion was highly desired. In the last few decades, membrane filtration, which primarily bases on size exclusion, is known as a promising candidate for the separation of emulsion containing micron and submicron size of oil droplets [1, 5–7]. The advantageous properties of membrane filtration can be mentioned as eco-friendly, high separation efficiency, low energy consumption, less chemical addition. However, a mainly practical drawback which limits the widespread application of filtration membrane for treating oily waste water was fouling by pore plugging of oil droplet [8]. Therefore, the enhancement of fouling resistance of membrane plays a vital role in application of filtration membrane for emulsion separation.

The modification of the membrane tends to graft a hydrophilic functional group on the membrane to develop the selectivity and permeability. In addition, the surface grafting also enhances fouling resistance of membranes. In many technologies including UV irradiation, plasma, polydopamine, addictive blending, chemical grafting, etc. The grafting by atom transfer radical polymerization (ATRP) was a promising method because of its advantage of permanent modification, controllable chain growth [9]. For example, Husson et al. used ATRP to graft several polymers to the surface of microfiltration and ultrafiltration membranes, which showed the decrease of molecular weight cutoff with increasing

polymerization time [9]. They also used ATRP to graft poly (acrylic acid) and poly (vinyl pyridine) to regenerated cellulose and PVDF membrane, respectively. The chain length of grafted polymer was varied by changing polymerization time [9].

Recently, some researches have devoted to the materials for exceptionally high permeability, which focused on oriented pore/channels in angstrom dimension which theoretically and experimentally ultrafast permeation [10–13]. For instance, oriented nanochannels such as carbon and metal hydroxide nanotubes that were vertically embedded in support matrices results in significantly high permeation flux of water in ultra/nano filtration [11,12]. Because of oriented channels, exceptionally large porosity, easily tunable pore size and structural diversity [14–17], metal-organic frameworks (MOFs) sound appealing for membrane materials. There have been some pioneer researches employed MOF for water filtration membrane. Li et al. fabricated ZIF-8-based membrane by an interfacial method [18]. A continuous thin selective layer on polyethersulfone support membrane increased the rose bengal rejection of the membrane (from 38.2% to 98.9%). The sacrifice of permeability was ascribed to the hydrophobic pore of ZIF-8. Liu et al. deposited UiO-66 on the outermost surface of an alumina hollow fiber by secondary growth method [19]. The prepared composite membrane revealed good rejection and higher permeability compared to commercially available membranes. These works pioneered promising utilization of MOFs in conjunction with a support membrane for liquid phase separation

More recently, we fabricated a filled UiO-66 composite membrane which showed excellent methylene blue rejection and exceptional permeability at low pressure. However, the interparticle voids among UiO-66 nanoparticles eventually cause the leakage of the small solutes. Therefore, in order to overcome this limitation, the grafting of a hydrophilic

functional group not only fill the interparticle voids but also increase the fouling resistance of original UiO-66 [20]. Therefore, grafted polymer is a potential way to increase both the efficiency and durability of the composite membrane.

In this chapter, UiO-66, one of the most stable MOFs to water and chemicals [15,21–24], was grafted by a hydrophilic poly(ethylene glycol) methacrylate (PEGMA) via ATRP method. The results showed that PEGMA was successfully grafted from UiO-66 nanoparticles while keeping the crystallinity of UiO-66. The composite membranes were fabricated by depositing PEGMA-*g*-UiO-66 enhanced the selectivity and the fouling resistance in comparison with UiO-66 based membranes.

3.2. Experimental

3.2.1. Materials

Zirconium tetrachloride ($ZrCl_4$) (purity > 99.9%) and terephthalic acid (purity > 99%) obtained from Sigma-Aldrich. N,N-Dimethylformamide (DMF) as a solvent was purchased from Wako Chemical Industries Ltd. These chemicals were utilized for UiO-66 nanoparticle preparation. A cellulose nitrate (CN) membrane (diam. 47 mm, pore size 0.1 μm, Whatman) was utilized as a support membrane. Copper (I) chloride (CuCl), Copper (II) chloride ($CuCl_2$), 2,2'-bipyridine were obtained from Wako Chemical Industries Ltd. Lubricant Ulvac Oil R-2 was used for nanoemulsion preparation. Span 60 and Tween 60 were utilized as surfactants, which were purchased from Kanto Chemical Co., Inc, and TCI chemical industry Co., Ltd, respectively. Deionized water was used throughout the experiments.

3.2.2. UiO-66 nanoparticle preparation

A $ZrCl_4$ solution was prepared by dissolving $ZrCl_4$ (0.45 g) in 90 mL of N,N-dimethylformamide (DMF). A solution of terephthalic acid as the ligand was prepared by dissolving 0.34 g in another 90 mL of DMF. Both solutions were prepared in inert atmosphere and reacted in a round bottom flask at ±°C for 24 h under stirring after adding 0.24 mL of deionized water, resulting in the dispersion of UiO-66 nanoparticles in DMF. Then, the dispersion was washed three times with DMF before soaking in methanol three days with changing methanol every one day. After that, UiO-66 nanoparticles were dried in a vacuum oven at 100 °C for 24 hours.

3.2.3. PEGMA-g-UiO-66 preparation

(2-Bromo-2-methyl) propionyloxyhexyltriethoxysilane as an initiator was grafted to surface hydroxyl groups of UiO-66 nanoparticles with the average size of 90 nm in the presence of ammonia. After that, ethylene glycol methacrylate was polymerized from the grafted initiator in the presence of $CuCl/CuCl_2$/2,2'-bipyridine. Thus obtained PEGMA-*g*-UiO-66 was washed and stored in DI water.

3.2.4. Composite membrane preparation

0.6 or 1.0 mg of PEGMA-*g*-UiO-66 and UiO-66 nanoparticles dispersed in 6.0 mL of water were deposited on CN support membranes at a suction pressure of 30 mbar by a micro pipette. After that, the pressure was kept for 5 min before maintaining at 100 mbar for 5 min. The membranes were washed with 100 mL of water prior to natural drying for characterization.

3.2.5. Nanoemulsion preparation

50 mg oil was added to 1.0 L of water in the presence of an equivalent mass of surfactant mixture at a given hydrophilic-lipophilic balance (HLB). The mixture was dispersed by a homogenizer at 9000 rpm for 10 min. After that, the oil/water emulsion was characterized by DLS measurement.

HLB of surfactant is an empirical expression, which was featured for the relationship between hydrophilic and lipophilic degree of surfactant. In this chapter Span 60 (HLB 4.7) and Tween 60 (HLB 14.9) were utilized. HLB values were varied by changing the composition of the surfactants following the equation

$$\%Tween60 = \frac{\left(HLB_{mixture} - 4.7\right)}{\left(14.9 - 4.7\right)} \times 100\% \qquad (3.1)$$

$$\%Span60 = 100 - \%Tween60 \qquad (3.2)$$

A range of HLB was investigated for determining the best value for nanoemulsion preparation. Besides, homogenization time and oil concentration were also examined.

3.2.6. Characterization

Functional groups on UiO-66 and PEGMA-*g*-UiO-66 surfaces were analyzed based on attenuated total reflectance infrared spectroscopy (ATR-IR, Perkin Elmer Spectrum 100 FT-IR) in the range of 400-1800 cm^{-1} using a diamond crystal. The crystalline structure of dried nanoparticles was analyzed by X-ray diffraction (XRD, Rigaku SmartLab) using Cu Kα radiation (λ=1.54 Å) at 40 kV and 30 mA in the range of $5° \leq 2\theta \leq 40°$. Thermal gravimetric analysis (TGA) was performed on Mettler Toledo DSC 820 under air atmosphere in the range of 30–800 °C at a heating rate of 5 °C/min.

The morphology of membranes was observed by scanning electron microscopy (SEM, Hitachi S-4100) at an accelerated voltage of 20 kV. The droplet size distribution in nanoemulsion was determined by dynamic light scattering (DLS) using Nano zetasizer from Malvern Instruments.

3.2.7. Nanoemulsion filtration

The filtration performance of membranes was evaluated based on a suction filtration setup, in which 200 mL of nanoemulsion (50 ppm) was filtered by a membrane at a differential pressure of 0.1 bar, the volume of permeate phase was examined after each 2.0 min. The concentration of oil in feed and permeate phases was determined by UV-Vis measurement.

3.3. Results and discussion

3.3.1. Characterization

Characterization of nanoparticles

Fig. 3.1 shows the ATR-IR spectrum of dried UiO-66 nanoparticles in the skeletal mode region. The spectrum exhibits typical peaks of UiO-66 reported in literature [25,26]. For instance, an intense doublet at 1574 and 1395 cm^{-1} for the in- and out-of-phase stretching modes of the carboxylate group, and bands at 475, 744 and 548 cm^{-1} for the bending of OH and CH mixed with Zr−O modes, and Zr-(OC) asymmetric stretching vibration, respectively. ATR-IR spectrum of the PEGMA-*g*-UiO-66 shows the peaks at 1720 cm^{-1}, which were attributed to the carbonyl group vibration. The monomer EGMA consists of $CH_2=CR_1R_2$ whose stretching vibration peak can be identified at 1638 cm^{-1} [27,28]. The

peak was absent in the spectrum of the PEGMA-*g*-UiO-66 suggesting that the monomer was completely polymerized or/and washed. Consequently, ATR-IR spectra indicated that PEGMA was successfully grafted from UiO-66.

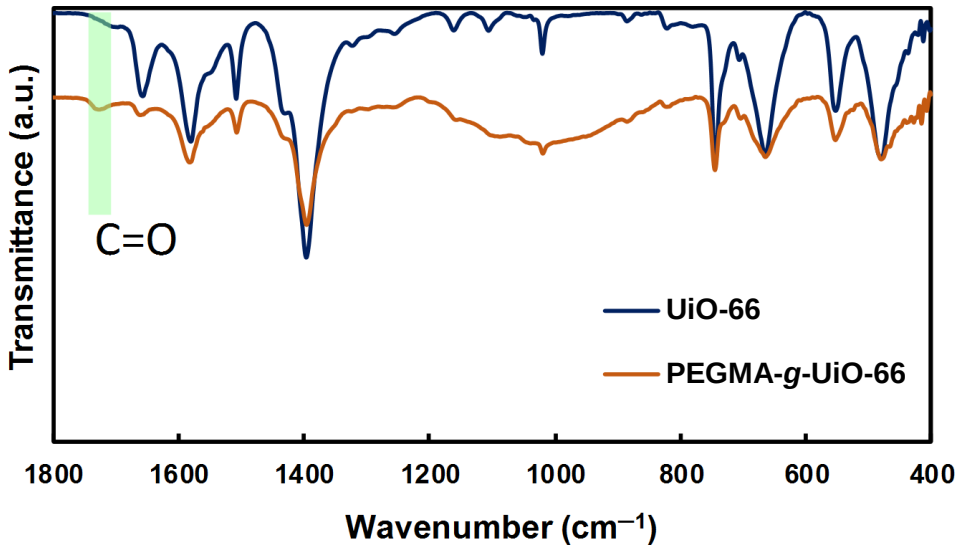

Fig. 3.1. ATR-IR spectra of UiO-66 and PEGMA-*g*-UiO-66

XRD patterns of dried UiO-66 nanoparticles (Fig. 3.2) also show consistent results with that in literature [22,29]: The diffraction peaks of the face-centered cubic (fcc) structure of UiO-66 crystals were well assigned. The peaks at 2-theta angles of 7.26, 8.39, 11.93, and 14.64° corresponding to the (111), (002), (022), and (222) planes. XRD patterns of original UiO-66 and PEGMA-*g*-UiO-66 show the consistency with each other, which suggested that the crystalline structure of MOFs remained after polymerization.

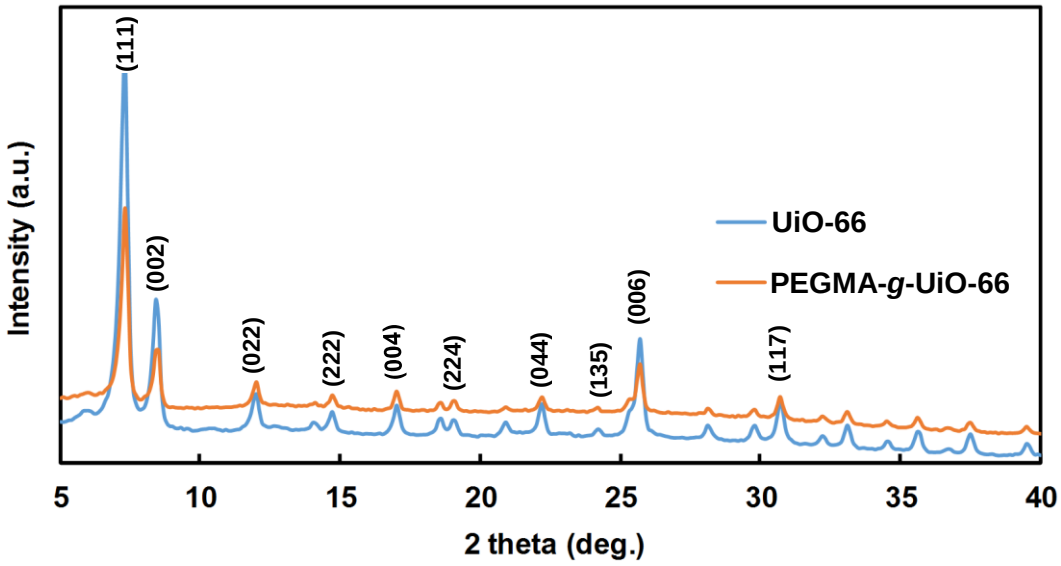

Fig. 3.2. PXRD patterns of UiO-66 and PEGMA-*g*-UiO-66 nanoparticles

The TGA results (Fig. 3.3) of UiO-66 nanoparticles show the decomposition at 520 °C, which is in accordance with literature [30,31]. In the presence of PEGMA, the decomposition curve of PEGMA-*g*-UiO-66 was different from the original ones. In oxygen atmosphere, at high temperature, the organic portions were completely decomposed and vaporized. The different weight loss of samples after TGA measurement exhibited the content of PEGMA grafted from the UiO-66 nanoparticles. The results show that the content of PEGMA in PEGMA-*g*-UiO-66 was about 11%.

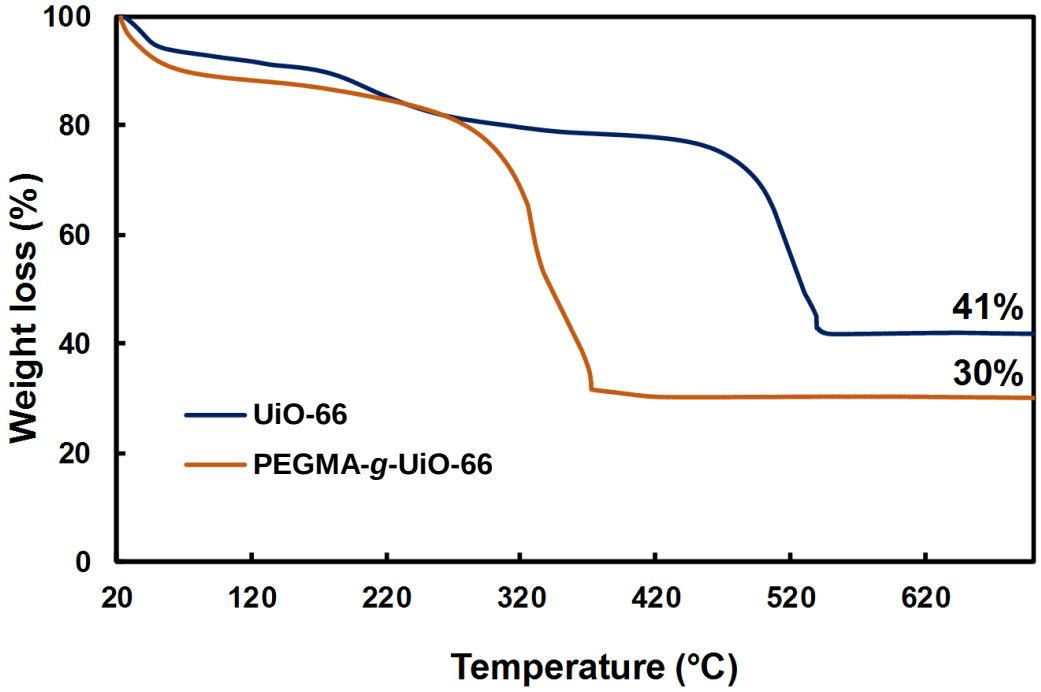

Fig. 3.3. TGA of UiO-66 and PEGMA-*g*-UiO-66

Characterization of the membranes

SEM images (Fig. 3.4) of the CN support membrane show a highly porous structure with the interlace of cellulose nitrate fibers. The inclusion of UiO-66 nanoparticles (0.6 mg) led to a thin layer formation on the CN membrane. However, the selective layer showed a high roughness morphology with many big cracks. The depositing of PEGMA-*g*-UiO-66 was unable to form a selective layer on the support membrane but distributed inside the porous structure of the support membrane (PEGMA-*g*-UiO-66-0.6 mg). The different of morphology of the membranes revealed the grafted PEGMA modified the nature of UiO-66 from less hydrophilic surface to more hydrophilic one. The less hydrophilic UiO-66 was rebelled by hydrophilicity of cellulose nitrate membrane leading to formation of a thin film. The higher hydrophilic surface of PEGMA-*g*-UiO-66 particle resulting in the adhesion of the particles to the cellulose nitrate fibers to form filled morphology.

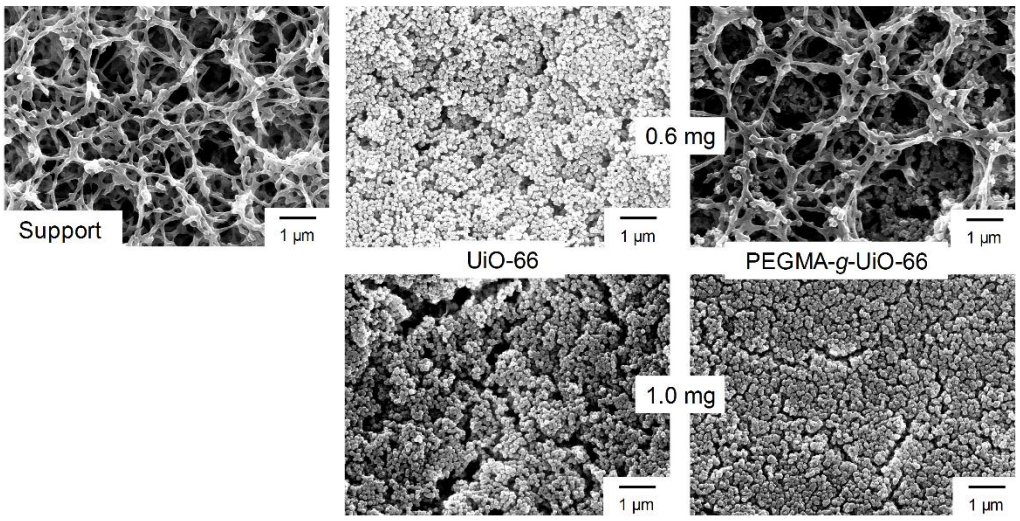

Fig. 3.4. SEM images of the membranes

Nanoparticle loading was increased to 1.0 mg of UiO-66 and PEGMA-*g*-UiO-66 leading to the formation of a selective layer in both cases. However, it was seen that the roughness of UiO-66 based membrane was higher than the other membrane. The difference of the roughness mainly due to the grafted polymer which developed the connection among nanoparticles to neighbor in comparison with non-grafted one. It was worth saying that UiO-66 particles were partially peeled off while PEGMA-*g*-UiO-66 particles were stable in washing process. This evidence revealed that grafted PEGMA enhanced the stability of the composite membrane.

3.3.2. Nanoemulsion filtration

Nanoemulsion preparation

Briefly, HLB of surfactant mixture was varied from 8 to 14.9 to determine the best HLB for emulsifying. Experimental results (not shown) revealed that the smallest droplet size was achieved at the HLB of 12 and the homogenization time of 10 min. Under these conditions, the droplet size of an emulsion of 50 ppm was evaluated as 71.5 ± 0.3 (Fig. 3.5).

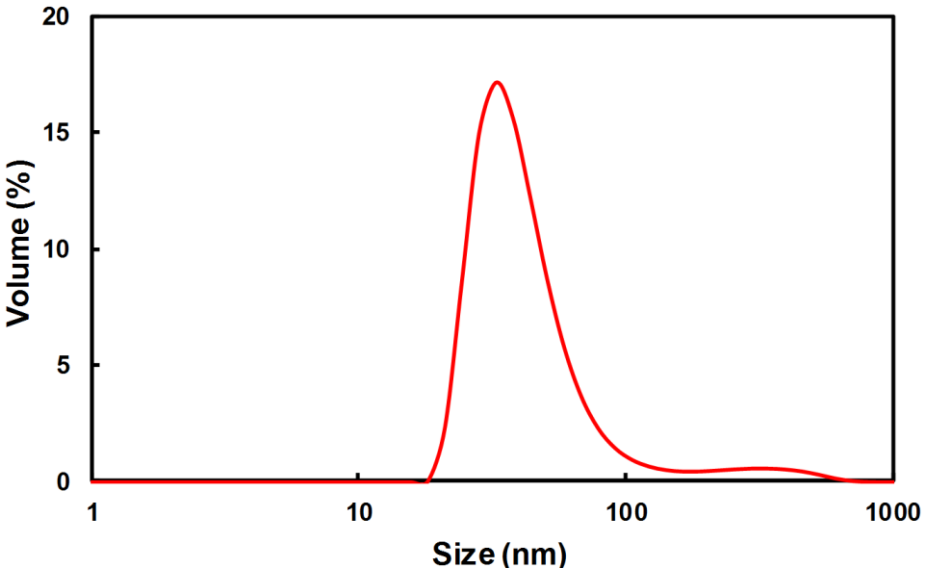

Fig. 3.5. DLS measurement of the oil/water emulsion

Nanoemulsion filtration

The selectivity of the membranes is shown in Fig 3.6a. As can be seen, the oil rejection for the support membrane was achieved as high as 74%. While, oil rejection of membranes UiO-66 and PEGMA-*g*-UiO-66 (0.6 mg) were 78.3 and 78.8%, respectively. This results suggested that the support membrane can partially remove oil from the emulsion, while the inclusion of a small amount of nanoparticles slightly increased the rejection. Fig. 3.6b shows the filtration performance of membranes UiO-66 and PEGMA-*g*-UiO-66 (1.0 mg). It was found that the selectivity significantly enhanced by increasing nanoparticle loading, the selectivity of these membranes was 94.7 and 97.7%, respectively. As can be seen in Fig. 3.6b, the selectivity of these membranes was kept constantly during the filtration. While, the permeability of both membranes tended to decrease because of fouling by the adhesion of oil on the surface of membrane.

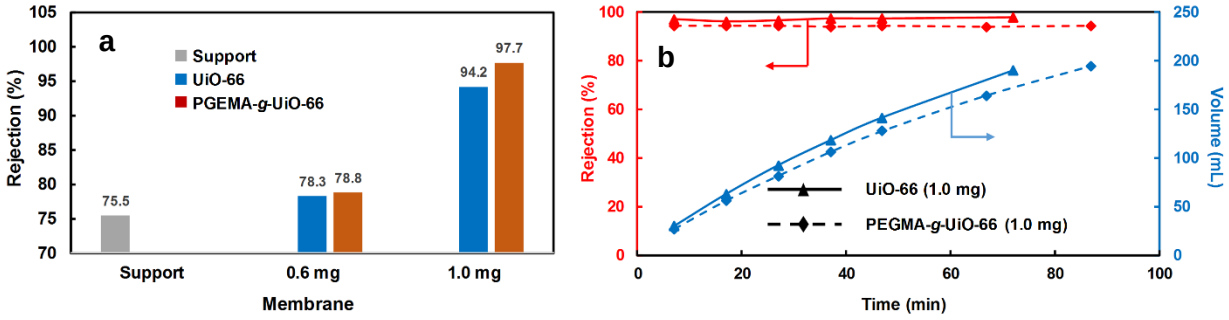

Figure 3.6. Oil/water emulsion filtration of the membranes

The flux losses of UiO-66 and PEGMA-*g*-UiO-66 (1.0 mg) membranes are shown in Fig. 3.7. It was found that the PEGMA-*g*-UiO-66-based membrane showed smaller flux loss than that of UiO-66-based membrane. Namely, after filtration of almost 200 mL of emulsion, the flux of UiO-66-based membrane decreased 61.0% while this value for PEGMA-*g*-UiO-66 membrane was 54.8%. This evidence implied that the inclusion of PEGMA improved the fouling resistance of the composite membrane.

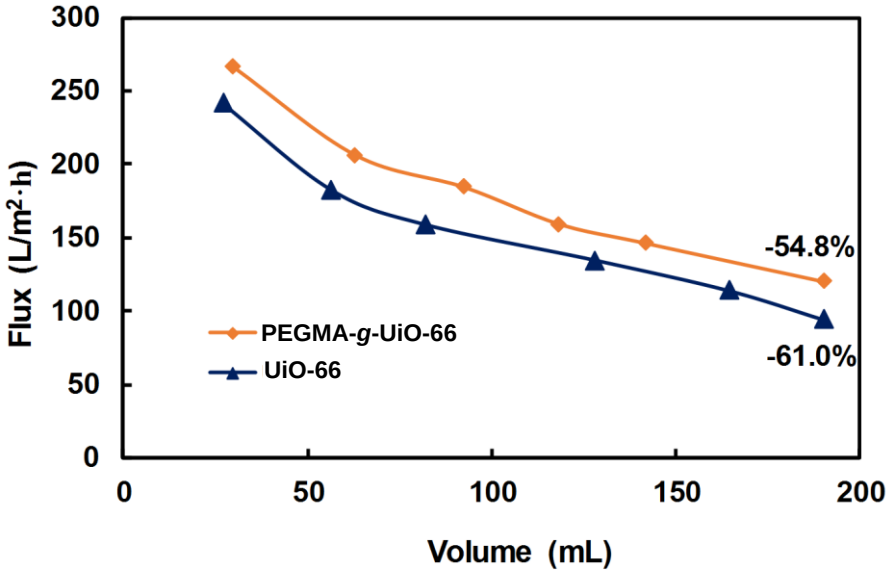

Fig. 3.7. Flux loss of membranes during filtration

3. 4. Conclusions

PEGMA was successfully grafted from UiO-66 nanoparticles. The XRD and TGA measurements exhibited that the crystalline structure of UiO-66 was retained during

polymerization, and the grafted amount of PEGMA was about 11%. The PEGMA-*g*-UiO-66 was used to deposit on the cellulose nitrate support. The composite membrane showed the increase in fouling resistance and selectivity compared to membrane prepared by original UiO-66 nanoparticles. Therefore, the grafted PEGMA not only increased the hydrophilicity of the composite membrane, but also partially filled the interparticle voids of the selective layer. It was believed that increase the amount of grafted PEGMA will enhance the filtration performance of the composite membrane.

3.5. References

[1] D. Qin, Z. Liu, H. Bai, D. D. Sun, X. Song, A new nano-engineered hierarchical membrane for concurrent removal of surfactant and oil from oil-in-water nanoemulsion, Sci. reports, 6 (2016) 24365.

[2] J. Liu, P. Li, L. Chen, Y. Feng, W. He, X. Lv, Modified superhydrophilic and underwater superoleophobic PVDF membrane with ultralow oil-adhesion for highly efficient oil/water emulsion separation, Mat. Lett. 185 (2016) 169–172.

[3] J. Zhang, Q. Xue, X. Pan, Y. Jin, W. Lu, D. Ding, Q. Guo, Graphene oxide/ polyacrylonitrile fiber hierarchical-structured membrane for ultra-fast microfiltration of oil-water emulsion, Chem. Eng. J. 307 (2017) 643–649.

[4] Q. Cheng, D. Ye, C. Chang, L. Zhang, Facile fabrication of superhydrophilic membranes consisted of fibrous tunicate cellulose nanocrystals for highly efficient oil/water separation, J. Memb. Sci. 525 (2017) 1–8.

[5] R. Muppalla, S.K. Jewrajka, A.V.R. Reddy, Fouling resistant nanofiltration membranes for the separation of oil–water emulsion and micropollutants from water, Sep. Purif. Technol. 143 (2015) 125–134.

[6] H. Ju, B.D. McCloskey, A.C. Sagle, Y-H. Wu, V.A. Kusuma, B.D. Freeman, Crosslinked poly(ethylene oxide) fouling resistant coating materials for oil/water separation, J. Memb. Sci. 307 (2008) 260–267.

[7] B.D. McCloskey, H. Ju, B.D. Freeman, Composite Membranes Based on a Selective Chitosan-Poly(ethylene glycol) Hybrid Layer: Synthesis, Characterization, and Performance in Oil-Water Purificatio, Ind. Eng. Chem. Res. 49 (2010) 366–373.

[8] J.S.B. Melbiah, D. Nithya, D. Mohan, Surface modification of polyacrylonitrile ultrafiltration membranes using amphiphilic Plutonic F127/$CaCO_3$ nanoparticles for oil/water emulsion separation, Colloid Surf. A: Physicochem. Eng. Asp. 516 (2017) 147–160.

[9] D. Miller, D. Dreyer, C. Bielawski, D. Paul, B. Freeman, Surface modification of water purification membranes: a review, Angew. Chem. Int. Ed. 56 (2016) 4662–4711.

[10] J.R. Werber, C.O. Osuji, M. Elimelech, Materials for next-generation desalination and water purification membranes, Nat. Rev. Mater. 1 (2016) 16018.

[11] J.H. Walther, K. Ritos, E.R. Cruz-Chu, C.M. Megaridis, P. Koumoutsakos, Barriers to superfast water transport in carbon nanotube membranes, Nano Lett. 13 (2013) 1910–1914.

[12] H. Huang, Z. Song, N. Wei, L. Shi, Y. Mao, Y. Ying, L. Sun, Z. Xu, X. Peng, Ultrafast viscous water flow through nanostrand-channelled graphene oxide membranes, Nat. Commun. 4 (2013) 2979.

[13] X. Peng, J. Jin, Y. Nakamura, T. Ohno, I. Ichinose, Ultrafast permeation of water through protein-based membranes, Nat. Nanotechnol. 4 (2009) 353–357.

[14] S. Qiu, M. Xue, G. Zhu, Metal-organic framework membranes: from synthesis to separation application, Chem. Soc. Rev. 43 (2014) 6116–6140.

[15] N. Yanai, S. Granick, Directional self-assembly of a colloidal metal-organic framework, Angew. Chem. Int. Ed. 51 (2012) 5638–5641.

[16] H.-C. “Joe” Zhou, S. Kitagawa, Metal–Organic Frameworks (MOFs), Chem. Soc.

Rev. 43 (2014) 5415–5418.

[17] W. Lu, Z. Wei, Z.-Y. Gu, T.-F. Liu, J. Park, J. Park, J. Tian, M. Zhang, Q. Zhang, T. Gentle III, M. Bosch, H.-C. Zhou, Tuning the structure and function of metal–organic frameworks via linker design, Chem. Soc. Rev. 43 (2014) 5561–5593.

[18] Y. Li, L.H. Wee, A. Volodin, J. a Martens, I.F.J. Vankelecom, Polymer supported ZIF-8 membranes prepared via an interfacial synthesis method, Chem. Commun. 51 (2015) 918–920.

[19] X. Liu, N.K. Demir, Z. Wu, K. Li, Highly Water-Stable Zirconium Metal-Organic Framework UiO-66 Membranes Supported on Alumina Hollow Fibers for Desalination, J. Am. Chem. Soc. 137 (2015) 6999–7002.

[20] D. X. Trinh, T.P.N. Tran, T. Taniike, Fabrication of new composite membrane filled with UiO-66 nanoparticles and its application to nanofiltration, Sep. Purf. Technol. 177 (2017) 249–256.

[21] N.C. Burtch, H. Jasuja, K.S. Walton, Water Stability and Adsorption in Metal − Organic Frameworks, Chem. Rev. 114 (2014) 10575−10612.

[22] J.H. Cavka, S. Jakobsen, U. Olsbye, N. Guillou, C. Lamberti, S. Bordiga, K.P. Lillerud, A New Zirconium Inorganic Building Brick Forming Metal Organic Frameworks with Exceptional Stability, 6 (2008) 13850–13851.

[23] L. Valenzano, B. Civalleri, S. Chavan, S. Bordiga, M.H. Nilsen, S. Jakobsen, K.P. Lillerud, C. Lamberti, Disclosing the complex structure of UiO-66 metal organic framework: A synergic combination of experiment and theory, Chem. Mater. 23 (2011) 1700–1718.

[24] F. Ragon, B. Campo, Q. Yang, C. Martineau, A.D. Wiersum, A. Lago, V. Guillerm, C. Hemsley, J.F. Eubank, M. Vishnuvarthan, F. Taulelle, P. Horcajada, A. Vimont, P.L. Llewellyn, M. Daturi, S. Devautour-Vinot, G. Maurin, C. Serre, T. Devic, G. Clet, Acid-functionalized UiO-66(Zr) MOFs and their evolution after intra-framework cross-linking: structural features and sorption properties, J. Mater. Chem. A. 3 (2015) 3294–3309.

[25] J.B. DeCoste, G.W. Peterson, H. Jasuja, T.G. Glover, Y. Huang, K.S. Walton, Stability and degradation mechanisms of metal-organic frameworks containing the $Zr_6O_4(OH)_4$ secondary building unit, J. Mater. Chem. A, 1 (2013) 5642–5650.

[26] J.B. DeCoste, G.W. Peterson, B.J. Schindler, K.L. Killops, M.A. Browe, J.J. Mahle, The effect of water adsorption on the structure of the carboxylate containing metal–organic frameworks Cu-BTC, Mg-MOF-74, and UiO-66, J. Mater. Chem. A, 1 (2013) 11922–11932.

[27] S. Belfer, Y. Purinson, R. Fainshtein, Y. Radchenko, O. Kedem, Surface modification of commercial composite polyamide reverse osmosis membranes, J. Memb. Sci. 139 (1998) 175-181.

[28] M. Poplawska, I. Schimpf, D. Brady, C. Kealey, A. Mulvihill, C.L. Higginbotham, Synthesis and characterization of polyethylene glycol dimethacrylate hydrogels for biomedical application, Applied Mechanics. Mater. 679 (2014) 158-170.

[29] M. Kandiah, S. Usseglio, S. Svelle, U. Olsbye, K.P. Lillerud, M. Tilset, Post-synthetic modification of the metal–organic framework compound UiO-66, J. Mater. Chem. 20 (2010) 9848–9851.

[30] M.J. Katz, Z.J. Brown, Y.J. Colon, P.W. Siu, K.A. Scheidt, R.Q. Snurr, J.T. Hupp,

O.K. Farha, A facile synthesis of UiO-66, UiO-67 and their derivatives, Chem. Commun. 49 (2013) 9449–9451.

[31] M. Kandiah, M.H. Nilsen, S. Usseglio, S. Jakobsen, U. Olsbye, M. Tilset, C. Larabi, E.A. Quadrelli, F. Bonino, K.P. Lillerud, Synthesis and Stability of Tagged UiO-66 Zr-MOFs, Chem. Mater. 22 (2010) 6632–6640.

Chapter 4

Development of reverse osmosis membranes based on UiO-66 nanoparticles deposited on polymeric support

4.1. Introduction

Recently, materials with oriented nanochannels/pores have been widely applied for filtration membranes. Nanochannel-based materials such as stacked graphene, carbon nanotubes (CNTs) and aquaporin endow membranes with the permeation flux of water from one to three orders of magnitudes higher than those of commercial membranes [1–3]. Surwade et al. created nanoscale pores in a layer of graphene by the oxygen plasma etching process and applied for desalination. The free standing membranes exhibited two orders of magnitudes permeability higher than that of commercially available membranes [4]. In a computational research on CNT membrane, Corry simulated water permeation through CNTs (7,7) with the diameter of 10 Å for desalination. The membrane exhibited over 1500 times of flux compared with those of existing membranes [5]. In another work, Holt et al reported that the permeability of sub-2-nanometer CNT membrane showed several orders of magnitudes higher than those of commercial membranes [6]. In the other case, the using of Aquaporin Z, a kind of pore forming protein in living cells,revealed 80 times permeability higher than those of the reverse osmosis (RO) membranes [7]. Because of their exceptional water transport, these classes of materials have been considered as next-generation materials for filtration membranes [3].

Owning to their advantages such as nanochannels, highly porous structure and easily tunable pore size, metal-organic frameworks (MOFs) sound a promising class of materials [8]. Ma et al. dispersed core-shell UiO-66@graphene oxide (GO) particles into polyethersulfone (PES) casting solution to fabricate UiO-66@GO/PES membranes for ultrafiltration. The inclusion of UiO-66 increased the hydrophilicity of GO/PES membranes. The permeability of the UiO-66@GO/PES membranes was 350% higher than those of PES membranes [9]. In another work, Sotto and cowokers blended MOF-74 with

PES before casting membranes. The MOF-based membrane showed an increase in porosity, permeability and antifouling ability compared to the neat PES membrane [10]. By applying an interfacial method, Li et al prepared a ZIF-8 layer on the PES substrate membrane and applied the membrane to ultrafiltration. The ZIF-8 layer significantly enhanced the selectivity of the membranes. However, because of the hydrophobic nature of ZIF-8, the flux of MOF-based membranes dropped remarkably [11]. More recently, Liu et al deposited UiO-66 on the outermost surface of alumina hollow fiber by secondary growth method, a 2 μm thick layer of UiO-66 rejected multivalent cations from water (98% for Mg^{2+}, 99.3% for Al^{3+}) based on size exclusion mechanism. On the other hand, the permeability of the membrane was 0.28 $L/m^2 \cdot h \cdot bar \cdot \mu m$ comparable to those of commercial polymeric RO membranes [12]. These promising results suggest that MOFs are emerging as excellent materials for water purification by membrane-based technology.

In chapter 2, a novel composite membrane was fabricated by depositing nanoparticles of UiO-66, one of the most stable MOFs, on a microfiltration membrane of regenerated cellulose. The membrane offered two pathways for water transport including intraparticle channels and interparticle voids. The results proved that nanochannels of UiO-66 were the main pathway for water transport, resulting in a perfect rejection of methylene blue from aqueous solution while keeping an excellent permeability and flexibility [13]. However, the interparticle voids among nanoparticles would eventually cause the leakage of small solutes. In order to address this drawback, the filling the interparticles voids for improving the performance of UiO-66 composite membranes is necessary and the selection of polyamide (PA) for this purpose is promising.

In general, the incorporation of nanoparticles in a PA selective layer has provided thin film nanocomposite (TFN) membranes [14–17]. The nanoparticles in TFN membranes

acts as a nano-filler to enhance performances such as water permeability [18,19], fouling resistance [20–22] of thin film composite (TFC) membranes, which were prepared without nanoparticles. In literature, the inclusion of nanoparticles on the selective layer can be achieved by an approach, in which nanoparticles were dispersed in either the aqueous phase or the organic phase before interfacial polymerization [23]. If nanoparticles were dispersed in the aqueous phase, the removal of excess liquid by rubber roller will partially remove the nanoparticles or/and cause the heterogeneity of the membrane. Because of high hydrophilicity, thus nanoparticles show a poor dispersion in the organic phase. As a result, the membrane shows agglomeration of nanoparticles in the selective layer [23–25]. In other words, this approach causes the biggest drawback of the TFN membrane and a rational route to enhance the uniform distribution of nanoparticles in PA layer has been expected.

In this chapter, I utilized interfacial polymerization to fill the interparticle voids of the UiO-66 nanoparticles deposited on a polyethersulfone (PES) support membrane by cross-linked polyamide, forming a PA/UiO-66/PES membrane. The immobilization of UiO-66 nanoparticles on the substrate membrane as well as the removal of excess liquid on the membrane by nitrogen gas provided a good approach to address the drawback of conventional TFN membranes. The results showed that uniform dispersion of UiO-66 nanoparticles was achieved and the PA/UiO-66/PES membranes can be applied to RO desalination with improved performance in both permeability and salt rejection over PA/PES. membranes. The increment of the permeability was most plausibly because of the contribution of UiO-66 nanochannels (6 Å) for water transport. The results in this chapter confirmed that the UiO-66 was a very promising candidate for development of RO membranes.

4.2. Experimental

4.2.1. Materials

Zirconium tetrachloride ($ZrCl_4$) (purity > 99.9%), terephthalic acid (purity > 99%) for UiO-66 nanoparticle preparation were purchased from Sigma-Aldrich. N,N-Dimethylformamide (DMF) as a solvent was purchased from Wako Chemical Industries Ltd. Polyethersulfone (PES) membranes (diam. 47 mm, pore size 0.22 μm,) utilized as support membranes were obtained from Millipore. 1,3-diphenylene diamine (MPD) (≥ 98%), trimesoyl chloride (TMC) (> 98%), triethylamine (TEA) (> 99%) and (+)–10–camphosulphonic acid (CSA) (> 98%) were purchased from Tokyo Chemical Industry Co., Ltd. Hexane (> 96%) was delivered from Kanto Chemical Co., INC. These chemicals were utilized for interfacial polymerization. Deionized water was used throughout the experiments.

4.2.2. Preparation of UiO-66 nanoparticles

$ZrCl_4$ (0.30 g) was dissolved in 90 mL of DMF and 0.22 g of terephthalic acid in another 90 mL of DMF. After mixing the two solutions, 0.18 mL of water was added, which acts as a modulator for enhancing the nucleation rate and controlling the distribution size of UiO-66 nanoparticles [13]. These steps were conducted under nitrogen. The mixture was reacted under stirring at 100 °C for 24 h in an inert atmosphere, resulting in a stable dispersion of UiO-66 nanoparticles in DMF. The UiO-66 nanoparticles were washed by soaking in methanol for 3 days in which methanol was replaced by fresh one every day. Finally, UiO-66 nanoparticles were stored in methanol in a refrigerator. In preparing membranes, the dispersion of UiO-66 in methanol was sonicated for 2 h, followed by

centrifugation at 2000 rpm for 10 min to remove aggregated nanoparticles. The resultant supernatant was used for the preparation.

4.2.3. Membrane preparation

UiO-66/PES composite membranes were prepared by a suction filtration setup according to the previously reported procedure [13]. Briefly, a PES support membrane was placed on a filter holder. 0.5 mg of UiO-66 nanoparticles dispersed in 0.25 mL of methanol was dropped on the top of the PES membrane at a differential pressure of 20 mbar. Then, the membrane was washed with 10 mL of DI water. Then the membrane was taped on a glass plate with the UiO-66 side exposed and soaked in an aqueous phase, which was prepared by dissolving MPD in water in the presence of 4.0 g of (+)–10–camphosulphonic and 2.0 g of TEA. After a predetermined time, the glass plate was taken out and the excess liquid on the membrane was completely removed by nitrogen flow. The membrane was soaked in an organic phase for a predetermined time, which was a solution of 0.1 w% of TMC in hexane. After that, the membrane was cured at 70 °C for 30 min in a constant temperature oven. The membrane was stored in water until use or characterization.

A reference membrane, called a PA/PES membrane, was prepared based on the above explained procedure, but in the absence of deposited UiO-66 nanoparticles.

Table 4.1. Conditions for PA/UiO-66/PES membrane preparation

Membrane name	MPD concentration (wt%)	UiO-66 loading (mg)	Time in aqueous phase (min)	Time in organic phase (seconds)
PA/UiO-66/PES-1	3	0.5	5	60
PA/UiO-66/PES-2	3	0.5	5	15
PA/UiO-66/PES-3	3	0.5	2	15
PA/UiO-66/PES-4	1	0.5	2	5
PA/UiO-66/PES-5	1	0.5	2	10
PA/UiO-66/PES-6	1	0.5	2	15
PA/UiO-66/PES-7	1	1.0	2	15

4.2.4. Characterization

Functional groups of UiO-66 nanoparticles and membrane surfaces were analyzed based on attenuated total reflectance infrared spectroscopy (ATR-IR, Perkin Elmer Spectrum 100 FT-IR) in the range of 450-1800 cm^{-1} using a diamond crystal. Transmission electron microscopy (TEM, Hitachi H7100) at an acceleration voltage of 100 kV was used to determine the size and morphology of UiO-66 nanoparticles. The UiO-66 dispersion was diluted 100 times in methanol and casted onto a TEM grid. The crystalline structure of dried UiO-66 nanoparticles was analyzed by X-ray diffraction (XRD, Rigaku SmartLab) using Cu Kα radiation (λ=1.54 Å) operating at 40 kV and 30 mA in the interval of $5° \leq 2\theta \leq 35°$.

The morphology of membranes was observed by scanning electron microscopy (SEM, Hitachi S-4100) at an accelerated voltage of 20 kV. The contact angles of membranes were obtained by a contact angle meter (Dropmaster DM-501, Kyowa Interface Japan) to evaluation the hydrophilicity of membranes. The contact angle was immediately measured after dropping 1.0 µm of DI water on top of membranes.

4.2.5. RO desalination

The RO desalination tests were conducted using handmade six identical dead-end stirred cells, which were connected to a tank of the feed solution (1000 ppm of NaCl in DI water). A membrane was placed in the filtration holder and preconditioned by filtering of DI water for 1 h at a differential pressure of 3.0 bar. After that, the feed solution was filtered under stirring at a differential pressure of 2.0 bar, which was generated by a nitrogen cylinder equipped with a pressure regulator. The concentration of NaCl in the feed and permeate solutions was determined by a conductivity meter.

Here, the filtration system is described in details, where six identical filtration cells offer a parallel filtration system (Fig. 4.1). A filter holder was designed for maximum pressure of 10 bar, feed volume per cell of 100 mL and an effective membrane area of 7.1 cm^2. Each filtration cells were equipped with a stirrer bar to avoid concentration polarization during filtration process. Experimental results showed that these filtration cells exhibited consistent filtration results in both permeability and selectivity for same membranes.

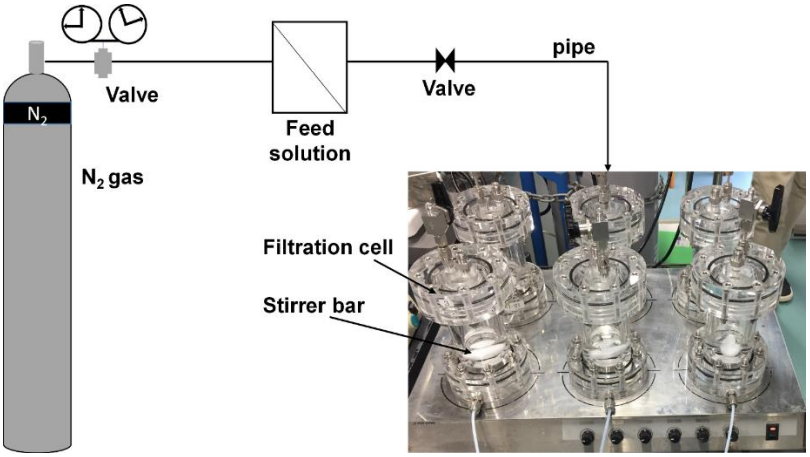

Fig. 4.1. High-throughput filtration system

The permeability (J) and the rejection (R) in the above desalination experiment was derived based on Eqs. (4.1) and (4.2), respectively.

$$J = \frac{V}{S \cdot \Delta P \cdot t} \qquad (4.1),$$

where: V is the permeate volume in L, S is the effective area of membrane in m^2, ΔP is the differential pressure in bar and t is the filtration time in h.

$$R = \frac{C_0 - C_p}{C_0} \times 100 \qquad (4.2),$$

where: C_0 and C_p are the concentrations of NaCl in the feed and permeate solution in mg/L, respectively.

4.3. Results and discussion

4.3.1. Characterization of UiO-66 nanoparticles

The characteristics of UiO-66 nanoparticles were carefully described in chapter 2. Briefly, Fig. 4.2a shows the ATR-IR spectrum of UiO-66 nanoparticles, which indicated the consistency with that in literature [26–28]. The doublet vibration peaks at 1574 and

1395 cm^{-1} were ascribed to the out-of-phase stretching modes of the carboxylate group. The vibration peaks at 475, 744 and 548 cm^{-1} were attributed to the bending of OH and CH mixed with Zr−O modes, and Zr-(OC) asymmetric stretching vibration, respectively. The absence of residue peaks confirmed a well washing process. Fig. 4.2b shows the XRD pattern of UiO-66, which was in accordance with the literature [12,29,30]. The diffraction peaks of the face-centered cubic (fcc) structure of UiO-66 crystals were well assigned. The peaks at 2-theta angles of 7.26, 8.39, 14.02 and 14.64° corresponding to the (111), (002), (022) and (222) planes. TEM image (Fig. 4.2c) of UiO-66 nanoparticles indicated the cubic shaped morphology with the average size of 50 nm. It is noteworthy that the morphology and size of the UiO-66 strongly depended on the water amount in reaction solution [31–33]. In general, water as a modulator accelerates the nucleation rate of $Zr_6O_4(OH)_4$ cluster thus the growth of crystals [13,31,33]. In fact, the presence of water shortened the reaction time with controllable particle size distribution.

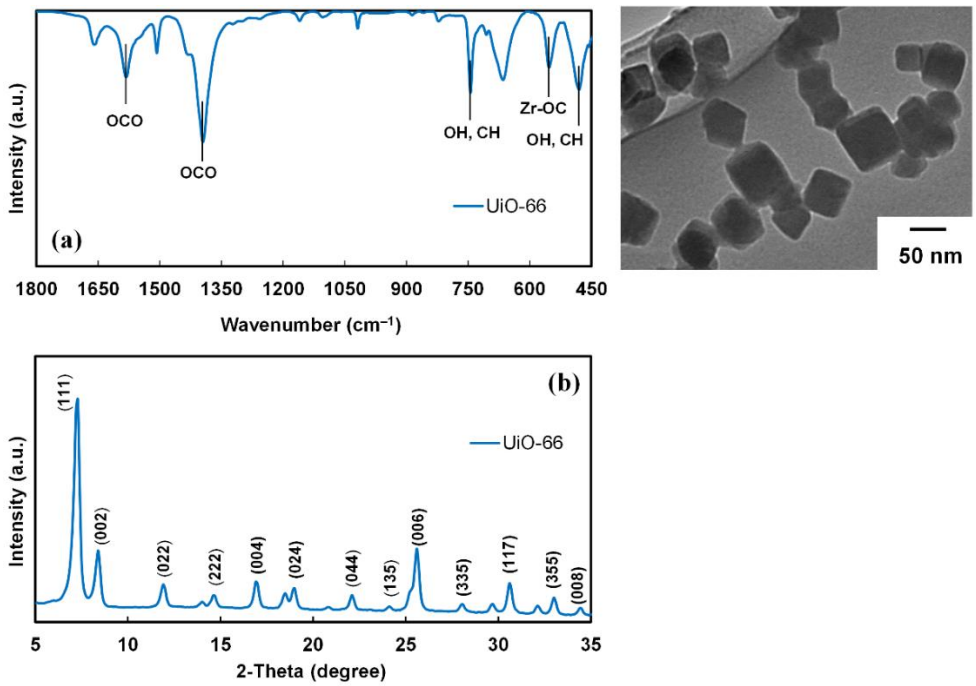

Fig. 4.2. Characterization of UiO-66 nanoparticles: a) FT-IR spectrum, b) XRD patterns, and c) TEM images

4.3.2. Characterization of membranes.

SEM images (Fig. 4.3) show that the PES support membrane has a porous morphology and large pores around 0.2 μm for microfiltration. Whereas, the composite UiO-66/PES membrane showed a morphology consisting UiO-66 nanoparticles deposited on top of the PES membrane. The crack formation was attributed to thermal stress originated from the drying process. SEM images showed dense morphology of the PA/PES and PA/UiO-66/PES-6 membrane surfaces, in which the SEM image of the PA/UiO-66/PES-6 membrane revealed the presence of UiO-66 nanoparticles. Compared to that of UiO-66/PES membrane, the PA/UiO-66/PES-6 membrane showed the integrity of the selective layer and all of interparticle voids among UiO-66 nanoparticles were filled by polyamide.

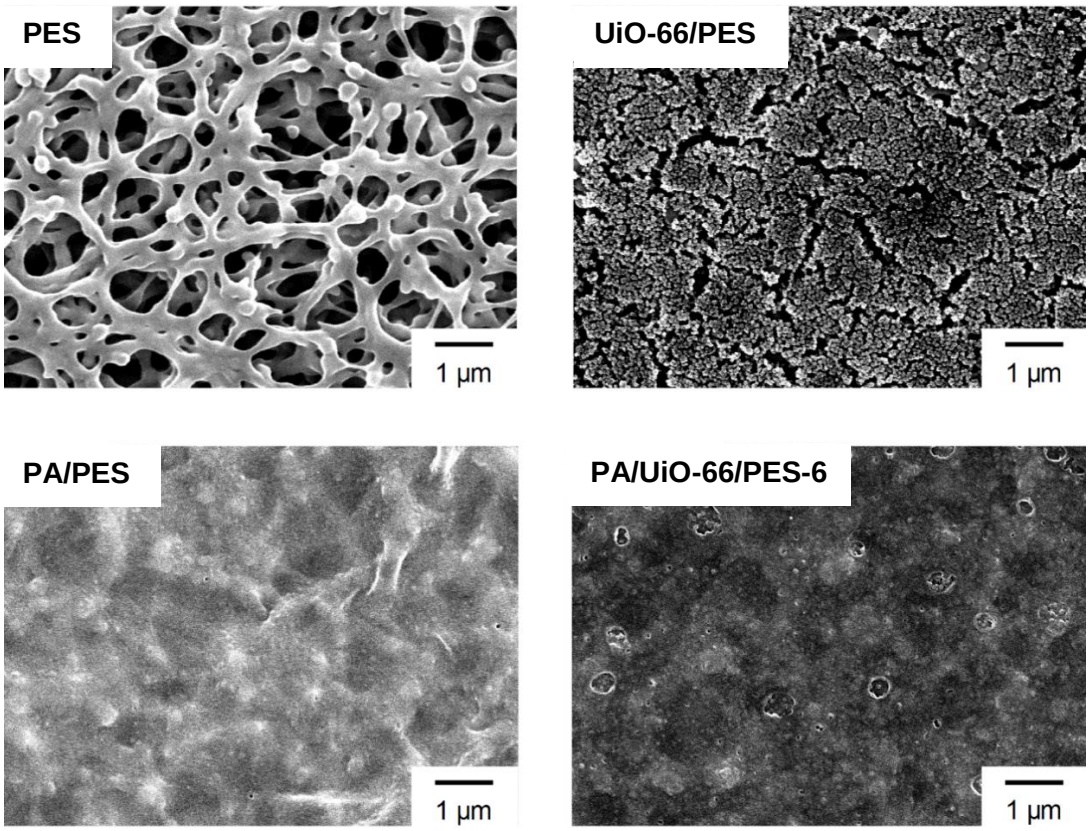

Fig. 4.3. SEM images of the membranes

It was found that the PA/UiO-66/PES-6 membrane possessed lower contact angle than that of the PA/PES membrane. It means that the presence of UiO-66 in the PA/UiO-66/PES-6 membrane increase the hydrophilicity in comparison with that of the TFC membrane. The contact angle of the PA/PES membrane was 59.4 ± 0.7, while the contact angles of the PA/UiO-66/PES membranes were 44.2 ± 0.1 and 28.7 ± 0.3 in the case of PA/UiO-66/PES-6 and PA/UiO-66/PES-7 membranes corresponding to the increase of UiO-66 loading from 0.5 and 1.0 mg, respectively. This increment in hydrophilicity was risen from more exposed of UiO-66 nanoparticles to the membrane surface corresponding to higher UiO-66 loading. This evidence suggested that UiO-66 nanoparticles enhanced the permeability of the membrane. As a result, the fouling resistance was also improved.

4.3.3. Desalination performance

The desalination performance of PA/UiO-66/PES membranes prepared by MPD 3% solution is summarized in Fig. 4.4. By decreasing the soaking time in the organic phase, the permeability of PA/UiO-66/PES-1 membrane increased from 0.31 to 0.42 $L/m^2 \cdot h \cdot bar$, corresponding to PA/UiO-66/PES-2 membrane. By decreasing the soaking time in aqueous phase from 5 min to 2 min, the permeability of membrane increased from 0.42 to 0.75 $L/m^2 \cdot h \cdot bar$, corresponding to permeability of PA/UiO-66/PES-2 and PA/UiO-66/PES-3, respectively. These increments were most plausibly because of the decrease in thickness of the polyamide in the selective layer.

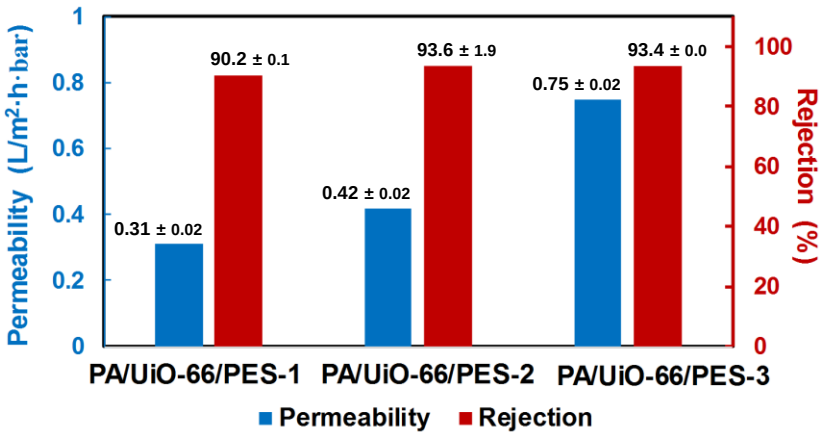

Fig. 4.4. Filtration performance of PA/UiO-66/PES membranes prepared by MPD 3%

RO desalination results of the membranes using MPD 1% solution are summarized in Fig. 4.5. The trend of permeability and salt rejection of the PA/UiO-66/PES-6 membrane are shown in Fig. 4.5a. It was found that the highest rejection and the permeability of the membrane were achieved at the first time of sampling (after 2 h). After that these values slightly reduced before retaining constantly. These results suggested that the RO desalination process reach a steady state after 2.0 h of filtration.

Fig. 4.5b indicates the influence of soaking time in the organic phase on the performance of the PA/UiO-66/PES membrane. It showed that the decease of the soaking time enhanced the permeability, which was most plausibly because of the decease of the thickness of the polyamide layer. However, the integrity of the selective layer may be slightly deteriorated leading to the decrease of the rejection. As can be seen, for 5 and 10 s of soaking time (PA/UiO-66/PES-3 and PA/UiO-66/PES-4, respectively), the salt rejection dropped significantly compared to the selectivity of the membrane soaked for 15 s (PA/UiO-66/PES-2) (67.3 and 94.3% for 10 and 15 s, respectively). In this sense, the critical condition for membrane preparation must be 15 seconds for soaking in the organic phase.

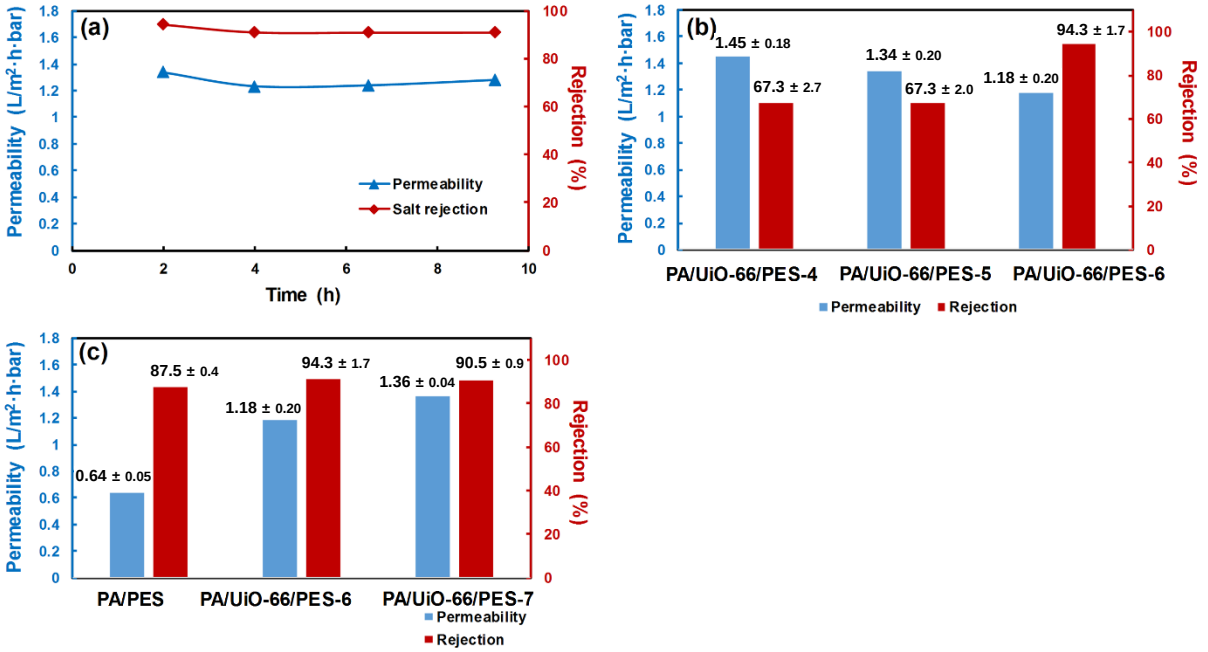

Fig. 4.5. Filtration performance of the membranes: a) the trend of performance by time, b) the effect of soaking time in the organic phase, and c) effect of the amount of UiO-66 on performance.

Fig. 4.5c shows the effect of the amount of UiO-66 nanoparticles on the filtration performance of the PA/UiO-66/PES membranes. The results revealed that the increase of UiO-66 amount led to the improvement of the permeability of membrane. At amount of 0 mg, corresponds to the PA/PES membrane and the permeability of the membrane was measured as 0.64 L/m^2·h·bar. The presence of 0.5 mg of UiO-66 nanoparticles significantly enhanced the permeability up to 1.18 L/m^2·h·bar. The permeability eventually reached 1.36 L/m^2·h·bar at 1.0 mg (PA/UiO-66/PES-7) while keeping comparably high salt rejection. The polyamide amount on these membranes was believed as similar. As a sequence, the increment of the permeability must be attributed to the enhanced hydrophilicity of the membranes by the inclusion of UiO-66 nanoparticles and/or the utilization of intraparticle channels of UiO-66 as an express pathway for water transport.

4.4. Conclusions

The interparticle voids of the UiO-66/PES composite membranes were filled by the polyamide based on the interfacial polymerization. The membranes were characterized by SEM technique. The results showed that UiO-66 nanoparticles were well distributed on the PA/UiO-66/PES membrane. It was notable that the poor distribution of nanoparticles is an inherent limitation in previous reports on TFN membranes. The membranes were applied for salt rejection by RO process. The PA/UiO-66/PES membrane exhibited a very good salt rejection, while the permeability was 200% higher than that of the PA/PES membrane. This increment was due to the increase of hydrophilicity in the presence of UiO-66 nanoparticles and/or the domination of intraparticle channels in water transport. These results revealed a very promising materials for water purification. In the future, I will continue research on the TFN membrane with the inclusion of $–NH_2$ functional groups, which may increase the compatibility with polyamide layer resulting in the better salt rejection.

4.5. References

[1] H. Huang, Z. Song, N. Wei, L. Shi, Y. Mao, Y. Ying, L. Sun, Z. Xu, X. Peng, Ultrafast viscous water flow through nanostrand-channelled graphene oxide membranes., Nat. Commun. 4 (2013) 2979.

[2] X. Peng, J. Jin, Y. Nakamura, T. Ohno, I. Ichinose, Ultrafast permeation of water through protein-based membranes, Nat. Nanotechnol. 4 (2009) 353–357.

[3] J.R. Werber, C.O. Osuji, M. Elimelech, Materials for next-generation desalination and water purification membranes, Nat. Rev. Mater. 1 (2016) 16018.

[4] S.P. Surwade, S.N. Smirnov, I.V. Vlassiouk, R.R. Unocic, G.M. Veith, S. Dai, S.M. Mahurin, Water desalination using nanoporous single-layer graphene, Nat. Nanotechnol. 10 (2015) 459–464.

[5] B. Corry, Designing Carbon Nanotube Membranes for Efficient Water Desalination, J. Phys. Chem. B. 112 (2008) 1427–1434.

[6] J.K. Holt, H.G. Park, Y. Wang, M. Stadermann, A.B. Artyukhin, C.P. Grigoropoulos, A. Noy, O. Bakajin, Fast mass transport through sub-2-nanometer carbon nanotubes, Science 312 (2006) 1034-1037.

[7] M. Kumar, M. Grzelakowski, J. Zilles, M. Clark, W. Meier, Highly permeable polymeric membranes based on the incorporation of the functional water channel protein Aquaporin Z, Proc. Natl. Acad. Sci. USA. 104 (2007) 20719–20724.

[8] S. Qiu, M. Xue, G. Zhu, Metal-organic framework membranes: from synthesis to separation application, Chem. Soc. Rev. 43 (2014) 6116–6140.

[9] J. Ma, X. Guo, Y. Ying, D. Liu, C. Zhong, Composite ultrafiltration membrane tailored by MOF@GO with highly improved water purification performance, Chem. Eng. J. 313 (2016) 890–898.

[10] A. Sotto, G. Orcajo, J.M. Arsuaga, G. Calleja, J.L. Aguirre, Preparation and characterization of MOF-PES ultrafiltration membranes, J. Appl. Polym. Sci. 132 (2015) 41633.

[11] Y. Li, L.H. Wee, A. Volodin, J.A. Martens, I.F.J. Vankelecom, Polymer supported ZIF-8 membranes prepared via an interfacial synthesis method., Chem. Commun. 51 (2015) 918–920.

[12] X. Liu, N.K. Demir, Z. Wu, K. Li, Highly Water-Stable Zirconium Metal-Organic Framework UiO-66 Membranes Supported on Alumina Hollow Fibers for Desalination, J. Am. Chem. Soc. 137 (2015) 6999–7002.

[13] D.X. Trinh, T. P.N. Tran, T. Taniike, Fabrication of new composite membrane filled with UiO-66 nanoparticles and its application to nanofiltration, Sep. Purif. Technol. 177 (2017) 249–256.

[14] B. Jeong, E.M.V. Hoek, Y. Yan, A. Subramani, X. Huang, G. Hurwitz, A.K. Ghosh, A. Jawor, Interfacial polymerization of thin film nanocomposites: A new concept for reverse osmosis membranes, J. Memb. Sci. 294 (2007) 1–7.

[15] M. Fathizadeh, A. Aroujalian, A. Raisi, Effect of added NaX nano-zeolite into polyamide as a top thin layer of membrane on water flux and salt rejection in a reverse osmosis process, J. Memb. Sci. 375 (2011) 88–95.

[16] M. Fathizadeh, A. Aroujalian, A. Raisi, M. Fotouhi, Preparation and characterization

of thin film nanocomposite membrane for pervaporative dehydration of aqueous alcohol solutions, Desalination, 314 (2013) 20–27.

[17] M. Ghanbari, D. Emadzadeh, W.J. Lau, S.O. Lai, T. Matsuura, A.F. Ismail, Synthesis and characterization of novel thin film nanocomposite (TFN) membranes embedded with halloysite nanotubes (HNTs) for water desalination, Desalination, 358 (2015) 33–41.

[18] X. Li, R. Wang, F. Wicaksana, C. Tang, J. Torres, A.G. Fane, Preparation of high performance nanofiltration (NF) membranes incorporated with aquaporin Z, J. Memb. Sci. 450 (2014) 181–188.

[19] N. Ma, J. Wei, R. Liao, C.Y. Tang, Zeolite-polyamide thin film nanocomposite membranes: Towards enhanced performance for forward osmosis, J. Memb. Sci. 405–406 (2012) 149–157.

[20] D. Emadzadeh, W.J. Lau, T. Matsuura, N. Hilal, A.F. Ismail, The potential of thin film nanocomposite membrane in reducing organic fouling in forward osmosis process, Desalination, 348 (2014) 82–88.

[21] D. Emadzadeh, W.J. Lau, M. Rahbari-Sisakht, A. Daneshfar, M. Ghanbari, A. Mayahi, T. Matsuura, A.F. Ismail, A novel thin film nanocomposite reverse osmosis membrane with superior anti-organic fouling affinity for water desalination, Desalination, 368 (2015) 106–113.

[22] J. Jagur-Grodzinski, Nanostructured polyolefins / clay composites: role of the molecular interaction at the interface, Polym. Adv. Technol. 17 (2006) 395–418.

[23] W.J. Lau, S. Gray, T. Matsuura, D. Emadzadeh, J.P. Chen, A.F. Ismail, A review on

polyamide thin film nanocomposite (TFN) membranes: History, applications, challenges and approaches, Water Res. 80 (2015) 306–324.

[24] V.A. Online, H. Huang, X. Qu, H. Dong, L. Zhang, H. Chen, Role of NaA zeolites in the interfacial polymerization process towards a polyamide nanocomposite reverse osmosis membrane, RSC Adv. 3 (2013) 8203–8207.

[25] J. Yin, E.S. Kim, J. Yang, B. Deng, Fabrication of a novel thin-film nanocomposite (TFN) membrane containing MCM-41 silica nanoparticles (NPs) for water purification, J. Memb. Sci. 423–424 (2012) 238–246.

[26] L. Valenzano, B. Civalleri, S. Chavan, S. Bordiga, M.H. Nilsen, S. Jakobsen, K.P. Lillerud, C. Lamberti, Disclosing the complex structure of UiO-66 metal organic framework: A synergic combination of experiment and theory, Chem. Mater. 23 (2011) 1700–1718.

[27] J.B. DeCoste, G.W. Peterson, H. Jasuja, T.G. Glover, Y. Huang, K.S. Walton, Stability and degradation mechanisms of metal-organic frameworks containing the $Zr_6O_4(OH)_4$ secondary building unit, J. Mater. Chem. A, 1 (2013) 5642–5650.

[28] J.B. DeCoste, G.W. Peterson, B.J. Schindler, K.L. Killops, M.A. Browe, J.J. Mahle, The effect of water adsorption on the structure of the carboxylate containing metal–organic frameworks Cu-BTC, Mg-MOF-74, and UiO-66, J. Mater. Chem. A, 1 (2013) 11922–11932.

[29] J.H. Cavka, S. Jakobsen, U. Olsbye, N. Guillou, C. Lamberti, S. Bordiga, K.P. Lillerud, A New Zirconium Inorganic Building Brick Forming Metal Organic Frameworks with Exceptional Stability, J. Am. Chem. Soc. 130 (2008) 13850–13851.

[30] M. Kandiah, S. Usseglio, S. Svelle, U. Olsbye, K.P. Lillerud, M. Tilset, Post-synthetic modification of the metal–organic framework compound UiO-66, J. Mater. Chem. 20 (2010) 9848–9851.

[31] Z. Hu, D. Zhao, De facto methodologies toward the synthesis and scale-up production of UiO-66-type metal–organic frameworks and membrane materials, Dalton Trans. 44 (2015) 19018–19040.

[32] Y. Bai, Y. Dou, L.-H. Xie, W. Rutledge, J.-R. Li, H.-C. Zhou, Zr-based metal–organic frameworks: design, synthesis, structure, and applications, Chem. Soc. Rev. 45 (2016) 2327-2367.

[33] B. Bueken, H. Reinsch, N. Reimer, I. Stassen, F. Vermoortele, R. Ameloot, N. Stock, C.E.A. Kirschhock, D. De Vos, A zirconium squarate metal–organic framework with modulator-dependent molecular sieving properties, Chem. Commun. 50 (2014) 10055–10058.

[34] C.J. Gabelich, J.C. Frankin, F.W. Gerringer, K.P. Ishida, I.H.M. Suffet, Enhanced oxidation of polyamide membranes using monochloramine and ferrous iron, J. Memb. Sci. 258 (2005) 64–70.

[35] S. Kao, S. Huang, D. Liaw, W. Chao, C. Hu, C. Li, D. Wang, K. Lee, J. Lai, Interfacially polymerized thin-film composite polyamide membrane : positron annihilation spectroscopic study , characterization and pervaporation performance, Polym. J. 42 (2010) 242–248.

Chapter 5

General conclusions

In this thesis, I employed UiO-66, one of the most stable metal-organic frameworks, which was supported on polymeric membranes and their application to nanofiltration, fouling resistance in oil/water emulsion separation and reverse osmosis desalination.

In **chapter 2**, a novel composite membrane was fabricated by depositing UiO-66 nanoparticles into the porosity of a regenerated cellulose membrane. The membrane was applied to remove methylene blue from its aqueous solution. The results indicated that the composite membrane can rejected 100% methylene blue, while keeping an exceptional water permeability. The experiment on adsorption of the membrane showed that the adsorption capacity of the composite membrane lower than that of the substrate membrane. As a results, the adsorption mechanism was excluded from the methylene blue rejection. Then, the fabrication a poreless TiO_2 membrane, which provided only interparticle voidss for water transport, showed that the membrane possessed a poor methylene blue rejection. Therefore, the interparticle voids never contributed to the methylene blue rejection. Consequently, these evidences proved that intraparticle channels in the UiO-66 nanoparticles were the major pathway for water transport. The investigation on polyethylene glycol rejection exhibited that the molecular weight cut-off of the composite membrane was in the range of 1.22-2.28 nm. I believe that, the results in **chapter 2** offer one of valuable contributions on the application nanochannel-based materials for filtration membranes, especially with flexibility, which dramatically enhanced the permeability of water, thus opening a potential choice to address the permeability-selectivity tradeoff of the conventional materials.

In order to enhance fouling resistance and performance of the composite membranes, in **chapter 3**, a hydrophilic poly(ethylene glycol) metacrylate (PEGMA) was grafted from UiO-66 nanoparticles before deposition on cellulose nitrate support membranes. The

composite membranes were applied to oil in water emulsion separation. The results showed that PEGMA was successfully grafted by atom transfer radical polymerization. ATR-IR spectrum of PEGMA-*g*-UiO-66 revealed the presence PEGMA on the UiO-66 nanoparticles, while TGA measurement showed that the grafted polymer content was about 11%. The PEGMA-*g*-UiO-66 membranes exhibited higher rejection of oil and higher fouling resistance in comparison with those of UiO-66-based membranes. These evidences exhibited that grafted PEGMA not only provided UiO-66 with higher fouling resistance but also partially filled interparticle voids among UiO-66 nanoparticles. In addition, while the grafting of polymer to MOF has been limited, I believe that the contribution of **chapter 3** was remarkable, which provides a potential choice for desired polymer grafting.

In order to completely fill the interparticle voids of the composite membranes mentioned in the previous chapters, **in chapter 4**, polyamide (PA) was employed to fill an UiO-66 layer on a polyethersulfone (PES) support membrane through interfacial polymerization, affording PA/UiO-66/PES membranes. By filling the interparticle voids, the membranes were applied for water desalination. The condition of polymerization was varied by changing concentration of m-phenylene diamine (MPD), UiO-66 loading, soaking time in aqueous and organic phases. The results exhibited that by decreasing the MPD concentration and the soaking time, the permeability of the PA/UiO-66/PES membranes increased most plausibly due to the decrease in PA layer thickness of the membranes. Contrary, the increase of UiO-66 loading increased the permeability of the membranes. These evidence suggested that UiO-66 nanoparticles provided a dominate contribution to membrane performance over PA. In comparison with PA/PES membranes, the PA/UiO-66/PES membranes with the same preparation condition exhibited higher salt rejection. Especially, the PA/UiO-66/PES membranes possessed 200% permeability higher, which

was explained by the increase of the hydrophilicity in the presence of UiO-66 and/or the contribution of the intraparticle channels for water transport.

I believe that the research work carried out in this thesis has established a novel and promising route to break through the limitations of current membranes. In general, in this dissertation I have solved few of the major challenges in the field of general membrane such as a) successful development a new composite membrane based on MOF-based discontinuous selective layer. The membrane overcame the tradeoff between permeability and selectivity, showing exceptional permeability and perfect selectivity while keeping the stability as well as flexibility, b) The dissertation also presented polymer grafting and filling strategies to improve the performance of the MOF-based membranes.

List of publications and other achievements

A) Publications

1. **Dai Xuan Trinh**, Thuy Phuong Nhat Tran, Toshiaki Taniike, "Fabrication of new composite membrane filled with UiO-66 nanoparticles and its application to nanofiltration", Separation and purification Technology, **2017**, 177, 249-256.

2. Linh Hoang Le, **Dai Xuan Trinh**, Trung Ba Le, Thuy Phuong Nhat Tran, Toshiaki Taniike, "Fabrication of functionalized graphene membrane for evaluation of permeation performance", Carbon, **2017,** 114, 519-525.

3. Thuy Phuong Nhat Tran, Ashutosh Thakur, **Dai Xuan Trinh**, Anh Thi Ngoc Dao, Toshiaki Taniike, "Design of Pd@Graphene Oxide Framework Nanocatalyst and its Application in Suzuki-Miyaura Cross-Coupling Reaction" (under review)

4. **Dai Xuan Trinh**, Thuy Phuong Nhat Tran, Thang Quoc Vu, Takashi Morinaga, Takaya Sato, Toshiaki Taniike, "Development of reverse osmosis membranes based on UiO-66 nanoparticles deposited on polymeric support" (Chapter 4) (In preparation)

B) International conferences

1. **Dai Xuan Trinh**, Toshiaki Taniike, "Ultrafast permeation composite membrane based on metal-organic framework for nanofiltration", International Conference on Materials Engineering and Functional Materials (ICMFM 2017), Hanoi, Vietnam, 8-10 May, **2017,** oral.

2. **Dai Xuan Trinh**, Toshiaki Taniike, “Development of reverse osmosis membrane based on UiO-66 nanoparticles deposited on polymeric support”, In ternational Conference on Membrane Science and Technology, Paris, France, 11-12 Sep., **2017,** oral.

3. Nhan Nu Thanh Ton, **Dai Xuan Trinh**, Kouichirou Katou, Takuma Ikenaga, Toshiaki Taniike “One-pot synthesis of a TiO2/graphene nanocomposite with outstanding photocatalytic capacity based on chemical exfoliation method", JAIST Japan-India Symposium on Materials Science 2017, Nomi, Japan, Mar. 6-7, **2017**, poster.

C) Domestic conferences

1. **Trinh Xuan Dai**, Toshiaki Taniike; “Metal-organic framework-based membrane applied for nanofiltration”, 64th Symposium on Macromolecules, Sendai, Japan, 15-17 Sep., **2015**, poster.

2. 関屋 有希, **Dai Xuan Trinh**, 谷池 俊明, "海水淡水化に関する RO 膜評価システムの開発", 平成 27 年度 日本化学会近畿支部 北陸地区講演会と研究発表会, 金沢, **2015** 年 11 月 27 日, ポスター発表

3. **Dai Xuan Trinh**, Toshiaki Taniike; “Ultrafast permeation composite membrane based on metal-organic framework for water filtration”, 65th Symposium on Macromolecules, Yokohama, Japan, 14–16 Sep, **2016**, oral.

4. **Dai Xuan Trinh**, Takashi Morinaga, Takaya Sato, Toshiaki Taniike, “Synthesis of poly(ethylene glycol) methacrylate-grafted UiO-66 nanoparticles and application for new composite membranes”, 66th Symposium on Macromolecules, May **2017**, poster.

5. Nhan Nu Thanh Ton, **Dai Xuan Trinh**, Kouichirou Katou, Takuma Ikenaga, Toshiaki Taniike, “Synthesis of TiO2/graphene nanocomposites for visible light photocatalyst based on chemical exfoliation method",日本化学会 第97春季年会, 横浜, **2017**年3月16-19日, 一般口頭.